Yellow adipocytes comprise a new adipocyte sub-type present in human bone marrow

Camille Attané[1#], David Estève[1#], Karima Chaoui[1], Jason Iacovoni[2], Jill Corre[3], Mohamed Moutahir[1], Philippe Valet[4], Odile Schiltz[1], Nicolas Reina[5, 6], Catherine Muller[1]

[1] Institut de Pharmacologie et de Biologie Structurale (IPBS), Université de Toulouse, CNRS, UPS, Toulouse, France

[2] Plateau de Bioinformatiques, Institut des Maladies Métaboliques et Cardiovasculaires (I2MC), Université de Toulouse, INSERM, UPS, Toulouse France

[3] Centre de Recherches en Cancérologie de Toulouse (CRCT), Université de Toulouse, INSERM, UPS, Toulouse, France

[4] Institut des Maladies Métaboliques et Cardiovasculaires (I2MC), Université de Toulouse, INSERM, UPS, Toulouse, France

[5] Département de Chirurgie Orthopédique et Traumatologique, Hôpital Pierre-Paul Riquet, CHU de Toulouse, Toulouse, France

[6] Laboratoire AMIS, UMR 5288 CNRS, Université Toulouse III-Paul Sabatier, Toulouse, France

# Contributed equally to this work

Corresponding author(s): Pr Catherine Muller**,** IPBS CNRS UMR 5089, 205 route de Narbonne, 31077 Toulouse Tel: 33-561-17-59-32; Fax: 33-561-17-59-33**;** e-mail: muller@ipbs.fr

Running title

Defect of lipolysis in bone marrow adipocytes

Abstract

During energy demanding conditions, white adipocytes store triglycerides and release fatty acids through lipolysis. In contrast, bone marrow adipocytes (BM-Ad) increase in size during caloric restriction, suggesting this fat depot exhibits precise metabolic specificity. We found subcutaneous adipocytes (SC-Ad) and BM-Ad share morphological features, but possess distinct lipid metabolism. BM-Ad show enrichment in cholesterol-oriented metabolism that correlates with increased free cholesterol content, while proteins involved in lipolysis were downregulated. A strong down-regulation in expression of monoacylglycerol (MG) lipase was observed leading to an accumulation of major MG species and accordingly the basal and induced lipolytic responses were absent in BM-Ad. These features are not recapitulated *in vitro* using differentiated bone marrow mesenchymal stem cells. Since our data demonstrate that BM-Ad comprise a distinct class of adipocytes, we propose renaming them yellow adipocytes.

Keywords

Bone Marrow adipocytes / cholesterol/lipolysis / monoacylglycerol lipase / proteomic

Introduction

In mammals, white adipose tissue (WAT) accumulates at various sites throughout the body. The most important and well-studied fat deposits occur in subcutaneous regions (SC-AT) and in the abdominal cavity surrounding key internal organs like the pancreas and intestines (Zwick et al, 2018). Other adipose-specific deposits also form around the heart, kidney, prostate in men and mammary glands in women (Zwick et al, 2018). In addition to WAT, mammals also possess brown adipose tissue (BAT) located in the interscapular and supraclavicular regions, representing less than 5% of the total fat mass (Leitner et al, 2017; Nedergaard et al, 2007; Saito et al, 2009; Zingaretti et al, 2009). Brown adipocytes participate in non-shivering thermogenesis and possess a specific morphology that includes several small lipid droplets and high mitochondria content (Bartelt & Heeren, 2014; Cinti, 2001). In contrast, white adipocytes store energy as triglycerides (TG) in their unique large lipid droplet (LD) after energy intake and release free fatty acids (FFA) through lipolysis in energy demanding conditions (Zechner, 2015). Lipolysis occurs through a biochemical pathway that uses consecutive actions of adipose triglyceride lipase (ATGL), which catalyzes the conversion of TG to diacylglycerols (DG) and hormone-sensitive lipase (HSL) and hydrolyzes DAG to monoacylglycerols (MG), monoacylglycerol lipase (MAGL) and the newly identified α/β hydrolase domain-containing protein 6 (ABHD6), which hydrolyzes MG to FA (Zhao et al, 2016) and glycerol (Zechner, 2015). White adipocytes also have an important endocrine function as they can release multiple soluble factors called adipokines, such as leptin and adiponectin (Fasshauer & Blüher, 2015).

One intriguing adipose tissue (AT) localizes to the bone marrow called bone marrow adipose tissue (BM-AT) that constitutes over 10% of the total fat mass in lean and healthy humans (Cawthorn et al, 2014). Technological advances in quantitative imaging of BM-AT in both mice and humans revealed that BM-AT presents unique features that highlight their physiological specificity. Many studies demonstrated that BM-AT increases in different pathophysiological conditions such as aging (Justesen et al, 2001; Scheller et al, 2015), osteoporosis (Justesen et al, 2001; Yeung et al, 2005) and obesity (Bredella et al, 2010; Doucette et al, 2015). These findings suggest this adipocyte population plays a larger role beyond that of "filler-cells". In stark contrast to the other WAT, the number and size of bone marrow adipocytes (BM-Ad) also increase during caloric restriction conditions in mice (Cawthorn et al, 2014; Devlin et al, 2010), rabbits (Bathija et al, 1979; Tavassoli, 1974) and human patients suffering from anorexia nervosa (Abella et al, 2002; Bredella et al, 2010). Decreases in bone marrow adiposity occurs only in severe nutrient deprivation in rabbits (Cawthorn et al, 2016) and late stages of anorexia nervosa associated with gelatinous transformation of the bone marrow (BM) [(Abella et al, 2002); for review (Ghali et al, 2016)].

Given the significant role for AT in regulating energy homeostasis, it is critical to elucidate why this tissue copes with changes in energy status in such a specific way that leads to still store and not dispense fuel when needed. However, knowledge of the phenotype of primary BM-Ad in physiology is sparse and hampered by difficulty to obtain sufficient isolated BM-Ad in mice and from harvesting human BM-AT partly due to the physical location (inside bone). Most studies on BM-Ad use rodents or human *in vitro* models. Mouse studies indicate BM-Ad regulate hematopoiesis and bone mass (Naveiras et al, 2009; Zhou et al, 2017). However, species-specific differences between rodent and human BM-AT exist that reinforce using caution when extrapolating information across species (Scheller et al, 2016). Two types of adipocytes in mouse have been described: regulatory and constitutive BM-Ad (rBM-Ad and cBM-Ad, respectively) (Scheller et al, 2015). cBM-Ad are present in tail vertebrae and the medullary canal from the tibia-fibular junction into the malleolus. However, rBM-Ad develop

postnatally within the BM of long bones extending from below the growth plate through the metaphysis and into the diaphysis (Scheller & Rosen, 2014). Existence of these two populations remains unconfirmed in humans. Inside the diaphysis of long bone, the number of BM-Ad varies between mouse strains and species, and some strains require pharmacological induction of BM-Ad by drugs such as glucocorticoids and thiazolidinedione (Scheller et al, 2016). Yet, human BM-Ad consistently fill 50 to 70% of the bone marrow cavity (Hindorf et al, 2010). Many studies use bone marrow mesenchymal stromal cells (BM-MSC) differentiated in adipocytes *in vitro*. However, it is unclear whether these differentiated cells recapitulate the phenotype of mature human primary BM-Ad. These *in vitro* studies suggest a role for BM-Ad in hematopoiesis regulation (Mattiucci et al, 2018; Naveiras et al, 2009), bone remodeling (Hardaway et al, 2015) and cancer progression (Diedrich et al, 2016; Herroon et al, 2013; Liu et al, 2015; Shafat et al, 2017; Tabe et al, 2017). These issues highlight that our knowledge of the physiological phenotype of primary BM-Ad remains limited. Using combined lipidomic and proteomic large-scale approaches, we purified and characterized human BM-Ad harvested from the femoral diaphysis of patients undergoing hip surgery with paired subcutaneous adipocytes (SC-Ad) and found that BM-Ad exhibit clearly distinct lipid metabolic features that reveal a new adipocyte sub-type.

Results/Discussion

Isolated SC-Ad and BM-Ad share morphological properties of white adipocytes.

After harvesting paired SC-AT and BM-AT from patients undergoing hip replacement surgery, we isolated adipocytes after collagenase digestion (Fig 1A). In AT from both locations, the vast majority of the space contained large and cohesive mature adipocytes with a unique LD filled with neutral lipids (assessed by Bodipy staining) (Fig 1B). Mature adipocytes from both locations expressed perilipin 1 (PLIN1) at the surface of the LD (Fig EV1A-B) and exhibited a very thin cytoplasm rim, a morphological trait expressed by white adipocyte (Fig EV1B) (Cinti, 2001). SC-AT and BM-AT also contained blood vessels highly positive for actin staining and stroma vascular cells at both stromal and perivascular positions (Fig 1B and Fig EV1A). Using transmission electron microscopy approach, we observed that both SC-Ad and BM-Ad present in the AT display a large LD surrounded by a very thin cytoplasm with the nucleus located at the cell periphery between the plasma membrane and the LD (Fig 1C). We performed an enzymatically based digestion protocol to isolate adipocytes from both tissues. After obtaining a population of cells constituted only of adipocytes, our results indicated that our tissue dissociation preserved the morphological identity of the isolated adipocytes. The isolated BM-Ad and SC-Ad shared the same morphology found within the tissues characterized by the presence of a unique and large LD filled with neutral lipids (Fig 1D). In addition, F-Actin staining showed a similar cytoskeleton architecture between the two types of cells (Fig 1D). Taken together, our results demonstrate the BM-AT present in the diaphysis of long bone is composed of cohesive adipocytes that exhibit the morphological appearance of white adipocytes as assessed by their unique LD, surrounded by a thin cytoplasm and a nucleus present at the periphery of the cells. With the caution noted in the introduction, a recent study in mice that used electronic transmission found that BM-Ad exhibit similar rounded morphology with a unique large LD (Robles et al, 2019). Yet, a recent report suggested that mouse BM-Ad express some genes related to BAT, including PRDM16 and FOXC2 (Krings et al, 2012). However, this study used whole tibia extracts, which contain adipocytes and contaminating cells, including myeloid cells and osteoblasts that express PRDM16 and FOXC2, respectively (Kim et al, 2009; Nishikata et al, 2011). Here, we present an initial morphological characterization of human BM-Ad, where they exhibit traits of white adipocytes that do not clearly distinguish them from "classical" white adipocytes.

Lipid profile in BM-Ad reveals enriched diverse lipid species like monoacylglycerol (MG) and cholesterol.

We then further characterized the phenotype of BM-Ad by studying their lipid profile compared to SC-Ad. Lipids were extracted from tissues and isolated adipocytes. As shown in Fig 2A, each tissue and isolated adipocytes showed a similar total lipid content. A quantitative LC-MS/MS based analysis of the total lipid content extracted from BM-Ad and SC-Ad was performed using a recently developed approach that uses both positive and negative ionization modes to cover the largest spectrum of detectable lipid species (Breitkopf et al, 2017). The analysis structurally characterized and identified 818 lipid species originating from the main lipid categories that belonging to 15 lipid classes. The majority of identified lipid species were glycerolipids (GL), including triacylglycerol (TG, 95 %) and diacylglycerol (DG, 2.1%). Beyond GL, the remaining lipids contain a large spectrum of phospholipids (PL), in particular phosphatidylcholine (PC, 1.9%), a major membrane constituent (Wen et al, 2018), sphingolipids (SL) and fatty esters (Fig 2B).

Unsupervised multivariate analyses of our lipidomic dataset indicated the variance between samples predominantly arose through inter-individual variability (Fig EV2A-B) indicating the lipids stored within mature

adipocytes likely came from food intake. We conclude that BM-Ad lipid composition reflects dietary lipid intake, which is consistent with a prior report in SC-Ad (Hodson et al, 2008). We then investigated if differences exist in lipid classes between SC-Ad and BM-Ad by comparing all quantified lipid species for one class between the two locations. As shown in Fig 2C, we observed differences in GL content. BM-Ad, in all samples, exhibited a slight increase in TG content with no changes in DG levels. MG content increased (Fig 2C), which reflected an increase of both saturated and unsaturated major MG species (Fig EV2C). These results suggest that the hydrolysis of MG is not efficient in BM-Ad. Two additional lipid classes are also increased in BM-Ad compared to SC-Ad, wax esters and sphingosine. Of note, only three sphingosine species were detected. The LC-MS/MS approach we used to quantify the lipid species does not identify cholesterol species, a key lipid species contained in adipocyte LD (Schreibman & Dell, 1975). Using a colorimetric assay, we found that BM-Ad showed a 1.5-fold increase in free cholesterol content compared to SC-Ad (Fig 2D). Cholesterol ester was not detected in either sample as we predicted since the vast majority of cholesterol is expressed in a free form in adipocytes (Schreibman & Dell, 1975). Here, we characterize the lipid content in BM-Ad using unsupervised lipidomic approaches. Inter-individual variability suggests that BM-Ad lipid content partially reflects dietary intake as in other adipose depots. Our results demonstrate that intrinsic differences exist between BM-Ad and SC-Ad regarding free cholesterol and MG contents.

Proteome of BM-Ad and SC-Ad differentiates adipocytes in lipid metabolic functions

We sought to further decipher the metabolic pathways specifically present in BM-Ad, so we conducted a large-scale proteomic analysis on paired SC-Ad and BM-Ad. We detail the data analysis general strategy in Fig EV3A. After data quality control, 3259 proteins were robustly detected. Interestingly, when we searched for proteins known to be secreted by adipocytes, termed adipokines (Fasshauer & Blüher, 2015), our dataset did not highlight significant differences between the two types of adipocytes and K-means clustering based on the expression pattern of adipokines did not allow clustering of the samples according to their anatomical location (Fig EV3B). BM-Ad expressed the adipocyte-specific adipokine, adiponectin, at the same levels as SC-Ad (Fasshauer & Blüher, 2015) (ADIPOQ, Table EV1). We obtained similar results for leptin (LEP, Table EV1), a hormone predominantly produced by adipocytes (Fasshauer & Blüher, 2015). These results indirectly assess the quality of cell preparation and their purity.

Among the 3259 proteins detected, 612 proteins involved in glucose and lipid metabolism were identified. We performed an unsupervised multivariate analysis focused on these proteins, which clearly demarcated the 4 samples according to their anatomical location (Fig 3A). The first two components of this analysis explained 41% and 20.8% of the dataset variance, respectively (Fig 3A). Statistical analysis of the 612 metabolic proteins differentially expressed in BM-Ad compared to SC-Ad identified 68 up-regulated proteins and 67 down-regulated proteins (Fig 3B). Pathway enrichment analysis with gene analytic software showed clear differences in the expression of proteins involved in several lipid metabolism pathways according to their anatomical locations (Fig 3C). Compared to SC-Ad, BM-Ad showed enrichment in arachidonic acid (AA) metabolism, SL signaling pathway and cholesterol metabolism delineated through cholesterol biosynthesis and statin pathways, while BM-Ad displayed downregulation of glucose and FA metabolism, as well as lipolysis regulation pathways (Fig 3C). Lipoprotein metabolism was also enriched and down-regulated in BM-Ad compared to SC-Ad (Fig 3C). In depth analysis of the proteins differentially expressed in this pathway revealed unexpected specificity for each fat depot.

We uncovered a clear separation of the samples by their location using hierarchical clustering dendrogram (Fig 3D). In BM-Ad, proteins involved in cholesterol transport (apoliproproteins APO-A2, -C1 and -C4) and hydrolysis, such NCEH1 (Neutral Cholesterol Ester Hydrolysis) and LIPA (Lipase A) (Litvinov et al, 2018), were enriched. This cholesterol-oriented metabolism in BM-Ad is strengthening by the enrichment of several proteins involved in cholesterol biosynthesis and statin pathways (Fig EV3C). On the opposite, proteins related to lipolysis were down-regulated in BM-Ad compared to SC-Ad in lipoprotein metabolism pathway (Fig 3D). Surprisingly, the lipases involved in TG hydrolysis LIPE (gene name of HSL) and MGLL (gene name of MAGL) were decreased (1. 19 ± 0.80, p= 0.016 for LIPE and -2.45 ± 0.35 p =0.00024 for MGLL, see Table EV1), as well as the Fatty Acid Binding Protein 4 (FABP4), one of the most abundant proteins in adipocytes that participate in maintaining adipocyte homeostasis and regulating lipolysis and adipogenesis (Prentice et al, 2019). Finally, BM-Ad and SC-Ad exhibited distinct expression patterns of proteins involved AA metabolism and FA metabolism (Fig EV3D-E). Despite similar morphology and expression pattern of adipokines, our results strongly support that BM-Ad are adipocytes that exhibit a very specific lipid metabolism compared to the "classical" SC-Ad. We uncovered an accumulation of free cholesterol in these cells. This conclusion is supported by unbiased proteomic approaches that indicate a seemingly unidentified cholesterol-oriented metabolism. In contrast to our results, a recent transcriptomic study comparing gene expression of human BM-Ad isolated from the femoral head and SC-Ad show that genes over-represented in human BM-Ad participate in signaling pathways without clear differences in the enzymes involved in lipid metabolism (such as cholesterol metabolism and TG hydrolysis) (Mattiucci et al, 2018). In addition, this report found decreased adiponectin expression, which stand in contrast to our current results and another study that identified BM-Ad as an important source of adiponectin (Cawthorn et al, 2014). We speculate technical issues, such as transcriptomic vs proteomic, and the different sources of BM-AT used may underlie the differences in these findings. We suspect that the specificity of BM-Ad in cholesterol metabolism may reflect their role in supporting BM hematopoiesis (Naveiras et al, 2009; Zhou et al, 2017). Cholesterol is essential constituent of the plasma membrane (Abe & Kobayashi, 2017) and could sustain cell division and plasma membrane fluidity and synthesis of surrounding hematopoietic cells that are under constant renewal. In contrast, the main functions of adipocytes, liberating energy reserve stores as TG under times of energy demand, appears downregulated in these cells. This interesting observation is consistent with the absence of a decrease in BM adiposity under energy deficit conditions (Bathija et al, 1979; Cawthorn et al, 2014; Devlin et al, 2010; Tavassoli, 1974). In particular, we observed a critical down-regulation of MAGL expression, a lipase required for the final hydrolysis of MG produced by HSL activation (Zechner, 2015). As such, MAGL deficiency in mice leads to a concomitant increase in MG levels in AT (Taschler et al, 2011) as observed in BM-Ad. The concomitant decrease of MAGL expression and increase in MG species strongly suggests that MAGL activity may be impaired in BM-Ad compared to SC-Ad.

Human primary BM-Ad present a defect in lipolytic activity not recapitulated in *in vitro* models

Due to the potential high impact of this newly described regulation in BM-Ad physiology, we further characterized the lipolytic pathway using Western blot analysis of the three major lipases involved in the consecutive hydrolysis of TG. While we observed no differences in ATGL and HSL expression in BM-Ad compared to paired SC-Ad, we found a sharp decrease (about 5-fold) in MAGL (Fig 4A). While we found a slight (1.21-fold) decrease in HSL protein expression in our proteomic studies, this result was not reproduced using Western blot analysis. This

discrepancy highlights inter-individual variability. We then functionally assayed lipolytic activity using *ex vivo* approaches on isolated adipocytes. Under basal conditions, we observed reduced glycerol and FFA release in BM-Ad compared to SC-Ad (Fig 4B and 4C). Under isoprenaline stimulation (a β-adrenergic agonist that serves as a strong lipolytic inductor) (Lafontan & Langin, 2009), we found no increase in glycerol (reflecting complete lipolytic reactions) or significant FFA release, but we did find a 3-fold increase in SC-Ad as expected (Lafontan & Langin, 2009). Thus, our data clearly demonstrate that human BM-Ad are devoid of lipolytic activity, which confirms their metabolic specificity.

A key finding from our study is the profound down-regulation of MAGL expression, which has never been reported for other AT. Strikingly, the two lipases ATGL and HSL possess several regulators of their activity involving interaction with other proteins as well as phosphorylation state under the control of hormones such as catecholamines (Lafontan & Langin, 2009). However, there is no evidence that cell energy status or hormones can influence MAGL activity, which renders it constitutively active (Lafontan & Langin, 2009). Since BM-Ad down-regulate MAGL expression, this indicates that these cells use the only efficient way to inhibit this specific activity. The slight, but not significant, increase of FFA upon lipolytic stimulation in BM-Ad (Fig 4C) suggests that the lipolysis process is not completely effective in these cells. In mice, a study suggests that rat cBM-Ad (from tail vertebrae) and rBM-Ad (from proximal tibia and femur) are resistant to lipolysis induced by β-adrenergic stimuli. This corresponds at the molecular level to a decrease in active phosphorylation of HSL, whereas the levels of ATGL and HSL remained unchanged compared to SC-Ad (Scheller et al, 2019). Such an additional regulatory process could also occur in human BM-Ad. Interestingly, the MAGL defect in BM-Ad is not compensated by ABHD6 expression, another lipase known to hydrolyze MG in visceral and brown AT but not in SC-AT (Zhao et al, 2016). ABHD6 expression levels remained constant between BM-Ad and SC-Ad in our proteomic study (Table EV1).

We then focused on the metabolic characteristic of BM-Ad we discovered, so we examined the physiological relevance of *in vitro* differentiated adipocytes used as the gold standard model for studying the role of BM-Ad. We differentiated human primary BM-MSCs and murine BM-MSC OP9 cell lines *in vitro* under adipogenic conditions. The murine pre-adipocyte 3T3-F442A served as a control reflecting "classical adipocytes". In all cells, the differentiation process strongly increased TG content (Fig 4D). *In vitro* differentiated adipocytes from BM-MSCs exhibited similar levels of basal lipolysis compared to differentiated 3T3-F442A (Fig 4E). Isoprenaline stimulation increased glycerol release in all cells studied (Fig 4E). These experiments demonstrated that adipocytes obtained from *in vitro* differentiation of human BM-MSCs do not recapitulate the functional defect in lipolysis observed in BM-Ad isolated from patients. We conclude from these results that *in vitro* differentiated BM-MSCs, considered the gold standard for studying BM-Ad functions, should be interpreted with high caution, since these cells do not recapitulate of key metabolic trait of the BM-Ad phenotype. The differentiation program of BM-Ad may exhibit distinct developmental gene expression patterns and epigenetic signatures that are not induced by the most widely used differentiation protocols that add PPARγ agonists (Lee & Fried, 2014; Ninomiya et al, 2010; Scott et al, 2011). We suggest that such protocols may artificially force BM-Ad progenitors towards a differentiation program into classical white adipocytes.

Conclusion

Here, we pioneered a methodology to characterize human primary BM-Ad using combined large-scale proteomic and lipodomic approaches. This approach revealed specific markers in a phenotype that refines and identifies BM-Ad. These cells morphologically resemble classical SC-Ad; however, we unraveled the specific lipid metabolism of BM-Ad, including the presence of a cholesterol-orientated metabolism that requires further investigation. We demonstrated altered lipolytic function in human primary BM-Ad due to a profound down-regulation of MAGL expression. This result underlies the differences in metabolic fitness upon caloric restriction between BM-AT and SC-AT. This specific phenotype is a previously unidentified feature of adipose depots that could explain why BM-AT behaves like a preserved lipid source, except during periods of extremely severe nutrient deprivation (Abella et al, 2002; Cawthorn et al, 2016). The specific function of this preservation, whether overall metabolic fitness or local interaction with proximal cells (such as hematopoietic cells), remains unknown. Adipocyte diversity continues to increase, so distinguishing markers and delineating specific phenotypes of these adipocyte subtypes gain importance. In addition to white and brown adipocytes, recent studies have identified beige adipocytes, an inducible form of thermogenic adipocytes (Zwick et al, 2018) and pink adipocytes in mouse mammary fat pad during pregnancy and lactation (Giordano et al, 2014). Given their specificity for lipid metabolism regardless of their morphological similarity to white adipocytes, we propose to define BM-Ad as a distinct type of adipocytes named “yellow adipocytes”.

Materials and Methods

Human subcutaneous and bone marrow tissue samples.

Paired subcutaneous (SC-AT) and bone marrow adipose tissue (BM-AT) were harvested from patients undergoing hip surgery in the Orthopedic Surgery and Traumatology Department of the Hospital Pierre Paul Riquet (Toulouse, France). All patients gave their informed consent and the samples were obtained according to national ethic committee rules (authorization° DC-215-2342). Briefly, during total hip replacement surgeries, after skin incision, maximus gluteus muscle and external rotators dissection, an osteotomy of the femoral neck was performed which allowed access to the intramedullary canal. While broaching the canal, BM-AT was aspirated cautiously with a soft cannula in the femoral proximal metaphysis and diaphysis before prosthesis placement. All procedures were performed using the same posterior approach. SC-AT were harvested using surgical blade at the incision site in the gluteal region. The samples were immediately placed in 37°C pre-warmed KRBHA (Krebs Ringer BSA HEPES Albumin buffer) corresponding to Krebs Ringer buffer (Sigma-Aldrich) supplemented with 100mM Hepes (Sigma-Aldrich) and 0.5% free fatty acid (FFA-free) bovine serum albumin (BSA) (Sigma-Aldrich) and rapidly carried out to the laboratory (within 1h) where they were processed. The BM-AT that share the same macroscopic aspects compared to SC-AT was dissected from area rich in hematopoietic cells (red marrow). For all the experiments performed in our study, 24 independent samples were used and obtained from 14 men and 10 women (mean age: 66.7 ± 13.9 years and mean body mass index (BMI): 26.8 ± 3.4 kg/m^2).

Adipocyte isolation.

SC-AT and BM-AT were rinsed several times in KRBHA prior to collagenase digestion (250 UI / mL diluted in PBS calcium and magnesium free supplemented with 2% FFA-free BSA (all products were obtained Sigma-Aldrich). After 30 min digestion at 37°C under constant shaking, samples were filtered with 100 and 200µm cell strainers (for BM-AT and SC-AT respectively) to remove cellular debris, undigested fragments and bone trabeculaes. The cell suspension was then gently centrifuged for 5 min at 200g at room temperature (RT). The floating adipocytes were then collected and rinsed with KRBHA several times to obtain a pure adipocyte cell suspension.

SC-AT and BM-AT confocal microscopy

Pieces of 0.5 cm² of whole SC-AT and BM-AT were fixed with a 4% paraformaldehyde solution (PFA, Electron Microscopy Sciences (EMS)) overnight. Fixed tissues were blocked and permeabilized in calcium and magnesium free PBS supplemented with 3% BSA and 0.2% Triton X100 (both obtained from Sigma Aldrich) for 1 h at RT. Tissues were then incubated overnight with a mouse anti PLIN1 serum (Acris Biosystem; 1:10 in calcium and magnesium free-PBS, 3% BSA, 0.2% Triton X-100). The following day the tissues were rinsed 5 times in PBS 0.05% Tween-20 and incubated for 2 h with a secondary antiboby coupled with CF488 dye (Biotum) for PLN1 staining, rhodamine coupled phalloidin (Thermofisher) for filamentous actin staining and TOPRO3® (Thermofisher) for nuclei staining. Z-stack images were acquired using LSM 710 confocal microscope and a 10X or 40X objective (Zeiss). Maximum intensity projection was made using Image J software and orthogonal views using Imaris software (v9.2; Bitplane).

Transmission electron microscopy

SC-AT and BM-AT were fixed with 2,5% glutaraldehyde and 2% PFA (EMS, Hatfield, PA, USA) in Cacodylate buffer (0.1M, pH 7.2) overnight at 4 °C and post-fixed at 4°C with 1% OsO4 and 1.5% K3Fe(CN)6 in the same buffer. Samples were treated for 1 h with 1% aqueous uranyl acetate and were then dehydrated in a graded ethanol series and embedded in EMBed-812 resin (EMS). After 48 h of polymerization at 60 °C, ultrathin sections (80 nm thick) were mounted on 75 mesh formvar-carbon coated copper grids. Sections were stained with 2% uranyl acetate (EMS) and 3% Reynolds lead citrate (Chromalys). Grids were examined with a TEM (Jeol JEM-1400, JEOL Inc) at 80 kV. Images were acquired using a digital camera (Gatan Orius, Gatan Inc, Pleasanton, CA, USA).

Confocal microscopy on isolated adipocytes

BM-Ad and SC-Ad were isolated as described above. Immediately after isolation, primary adipocytes were embedded in a fibrin gel to maintain cellular integrity. Briefly, 30µl of isolated adipocytes were gently mixed with 30µl of a fibrinogen solution (18 µg/mL in 0.9% NaCl buffer, Sigma-Aldrich) and 30µl of thrombin (3 units in 30µl of $CaCl_2$ solution, Sigma-Aldrich). Gel polymerization occurs rapidly at 37°C. The gels containing the primary adipocytes were fixed in 4% PFA for 1h and incubated with 10 ng/mL of Bodipy® 493/503, rhodamine coupled phalloidin and TOPRO3 (all products were obtained from Thermofischer). Samples were examined using LSM 710 confocal microscope and a 40X objective (Zeiss). Maximum intensity projection was performed using Image J software.

Lipidomic analysis

For the lipidomic and proteomic studies, 4 samples were used (2 men and 2 women, mean age: 67± 7. 4 years; mean BMI: 26.5 ± 3.1 kg/m^2). After 3 washes with PBS, isolated adipocytes (400 µl) were mixed 1.5 mL methanol in glass tubes. Sample mixture was then incubated with 5 mL of methyl tert-butyl ether (MTBE ;Sigma-Aldrich) for 1h at RT under gently shaking. After adding 1.2 mL of water, samples were centrifuged for 10 min at 1000 g. Upper phase (containing lipids) was transferred in a new glass tube. Lower phase was re-extracted with 2 volume parts of MTBE: methanol: water (10: 3: 2.5) and samples were centrifuged for 10 min at 1000 g and used for proteomic analyses (see below). Upper phase was collected, combined with the one collected after the first extraction and kept at -80°C for lipidomic analysis**.** One ml of lipid phase was evaporated under a nitrogen stream. Dried samples were sent to the Harvard mass spectrometry core and were analyzed by their untargeted lipidomics profiling platform. Lipids were resuspended with 100µl of 1:1 LC/MS grade isopropanol: acetonitrile methanol and 5 µl were injected onto the LC-MS/MS. Data acquisition was performed as previously described (Breitkopf et al, 2017). Briefly, each peaks area was calculated in both positive and negative ionization mode. The peaks allowing to structurally resolving the same lipid species were sum, if obtained from the same ionization. Only the lipid species detected at least in 3 samples from the same location were considered as robustly detected and used for the analysis. Missing values were imputed as the first percentile of the entire dataset. Then, values were log2 transformed and normalized with the function NormalizeBetweenArrays from Bioconductor package to perform the principal component analysis with R software (v3.5) and FactomineR package. The heatmaps and associated hierarchical clustering build on K-means methods were resolved with R software and ggplot2 package after centering the data around zero. The lipid species belonging to the same classes were sum to measure their relative

abundance and the log2 fold change of signal intensities for each class was calculated to compare the lipid classes between adipocyte locations. Violin plot was drawn with vioplot function in R.

Cholesterol content quantification

Cholesterol content within isolated adipocytes was measured using cholesterol assay kit (obtained from Abcam-ab65390) according to manufacturer recommendations. Briefly, lipids were extracted from isolated adipocytes using MTBE as described above. Free cholesterol and total cholesterol was sequentially quantified using colorimetric method. Optical density was determined at 570 nm with µ-quant spectrophotometer (BioTek Instruments).

Proteomic analysis

After 3 washes with PBS, proteins from isolated adipocytes (400µl) were purified with 5 mL of MTBE as described in lipidomic analysis section. Lower phase was centrifuged for 10 min at 5000 g at RT and pellet (containing proteins) was washed 2 times with PBS to remove solvents. Pellets were then resuspended with PBS 2% SDS, sonicated for 20 seconds and protein concentration was determined with the commercial kit (DC™ Protein Assay; Bio-Rad). Fifteen µg of proteins were reduced with modified Laemmli buffer (40 mM Tris pH 6.8, 2% SDS, 10% glycerol, 25mM DTT and 0.01% bromophenol blue) for 15 min at 65°C and alkylated by addition of 90mM iodoacetamide for 30 min at RT in the dark. Protein samples were loaded on a 1D SDS-PAGE gel (0.15 x 8 cm) and the electrophoretic migration was stopped as soon as the proteins entered the separating gel, in order to isolate all proteins in a single gel band (stained with Coomasie blue). The corresponding gel slice was excised and washed with 100 mM ammonium bicarbonate buffer. Proteins were in-gel digested using 0.6 µg of modified sequencing grade trypsin (Promega) in 50 mM ammonium bicarbonate overnight at 37°C. The resulting peptides were extracted in 50 mM ammonium bicarbonate followed by 10% formic acid/acetonitrile (1/1 v/v). The peptidic fractions were dried under speed-vacuum and resuspended with 5% acetonitrile, 0.05% trifluoroacetic acid (TFA) for MS analysis.

Peptides were analyzed by nanoLC-MS/MS using an UltiMate 3000 RSLCnano system coupled to a Q-Exactive Plus mass spectrometer (Thermo Fisher Scientific, Bremen, Germany). Five µL of each sample were loaded on a C-18 precolumn (300 µm ID x 5 mm, Thermo Fisher) in a solvent made of 5% acetonitrile and 0.05% TFA and at a flow rate of 20 µL/min. After 5 min of desalting, the precolumn was switched online with the analytical C-18 column (75 µm ID x 15 cm, Reprosil C18) equilibrated in 95% solvent A (5% acetonitrile, 0.2% formic acid) and 5% solvent B (80% acetonitrile, 0.2% formic acid). Peptides were eluted using a 5 to 50% gradient of solvent B over 300 min at a flow rate of 300 nL/min. The Q-Exactive Plus was operated in a data-dependent acquisition mode with the XCalibur software. MS survey scans were acquired in the Orbitrap on the 350-1500 m/z range with the resolution set to a value of 70000. The 10 most intense ions per survey scan were selected for HCD fragmentation and the resulting fragments were analyzed in the Orbitrap with the resolution set to a value of 17500. Dynamic exclusion was employed within 30 seconds to prevent repetitive selection of the same peptide. Duplicate technical LC-MS measurements were performed for each sample.

Raw mass spectrometry files were processed with the MaxQuant software (version 1.6.3.4) for database search with the Andromeda search engine and quantitative analysis. Data were searched against human entries of the Swissprot protein database (UniProtKB/Swiss-Prot Knowledgebase release 2018_02). Carbamidomethylation of

cysteines was set as a fixed modification whereas oxidation of methionine and protein N-terminal acetylation were set as variable modifications. Specificity of trypsin digestion was set for cleavage after K or R, and two missed trypsin cleavage sites were allowed. The precursor mass tolerance was set to 20 ppm for the first search and 4.5ppm for the main Andromeda database search. The mass tolerances MS/MS mode was set to 0.5 Da. Minimum peptide length was set to seven amino acids, and minimum number of unique peptides was set to one. Andromeda results were validated by the target-decoy approach using a reverse database at both a peptide and a protein FDR of 1%. For label-free relative quantification of the samples, the "match between runs" option of MaxQuant was enabled with a time window of 0.7min, to allow cross-assignment of MS features detected in the different runs.

The "LFQ" metric from the MaxQuant "protein group.txt" output was used to quantify proteins. Missing protein intensity values were replaced by a constant noise value determined independently for each sample as the lowest value of the total protein population. Only proteins identified in at least three samples in the same location (i.e. SC-Ad or BM-Ad) were considered as robustly detected and were used for statistical and bioinformatic analyses. Protein involved in lipid and glucose metabolism were selected using gene analytics software based on their involvement into the following pathways: Regulation of lipid metabolism; Insulin signaling-generic cascades; Lipoprotein metabolism; Adipogenesis; Regulation of lipid metabolism by Peroxisome proliferator-activated receptor alpha; Glucose / Energy Metabolism; Peroxisomal lipid metabolism; Calcium (Ca), cyclic adenosine monophosphate (cAMP) and Lipid Signaling; Nuclear Receptors in Lipid Metabolism and Toxicity; SREBF (Sterol Regulatory Element Binding Protein Gene) and miR33 in cholesterol and lipid homeostasis; Acyl chain remodeling of Phospho Ethanolamine (PE) ; Cholesterol and Sphingolipids transport / Distribution to the intracellular membrane compartments; Synthesis of substrates in N-glycan biosynthesis; Synthesis of Phosphatidyl Choline (PC); Metabolism of steroid hormones; Glycerophospholipid biosynthesis; Glucose metabolism; Fat digestion and absorption; Regulation of cholesterol biosynthesis by SREBP (Sterol Regulatory Element Binding Protein); cholesterol biosynthesis III (via desmosterol); Cholesterol and Sphingolipids transport / Transport from Golgi and ER to the apical membrane; Aldosterone synthesis and secretion; Citrate cycle (Tricarboxylic Acid (TCA) cycle); Adipocytokine signaling pathway; Sphingolipid metabolism; Fatty acid metabolism; Pyruvate metabolism; Arachidonic acid metabolism; Linoleic acid metabolism; Ceramide Pathway; Sphingolipid signaling pathway; sphingomyelin metabolism/ceramide salvage; Pentose phosphate pathway; Regulation of lipolysis in adipocytes; Mitochondrial Long Chain-Fatty Acid, Beta-Oxidation SuperPath; Fatty acid biosynthesis. Among the 1948 proteins retrieved by the database, we robustly identified 612 proteins. The label free quantification (LFQ) intensity for each identified protein was log2 transformed and used to perform the principal component analysis with R software (v3.5) and FactomineR package. The statistical analysis of differentially expressed proteins was performed with LIMMA package from Bioconductor using linear model followed by borrowing strength across protein with empirical bays methods with a design matrix build on two groups (BM-Ad and SC-Ad) (see Supplementary Table 1). The protein expression was considered significantly different if the p-value was lower than 0.05. Pathway enrichment analysis was performed with gene analytics software. The official gene symbol of the proteins significantly enriched or down-regulated was used as entry to determine the pathways enriched or downregulated respectively. The heatmaps and associated hierarchical clustering build on K-means methods were resolved with R and ggplot2 package.

***In vitro* adipogenesis**

The pre-adipocyte 3T3 F442A obtained from ECACC (00070654) were grown and differentiated into adipocyte as previously described (Meulle et al, 2008). OP9 cell were obtained from ATCC (ATCC CRL-2749). OP9 cells were seeded at $1x10^5$ cell/well in 6-well plates for 2 days in MEM alpha supplemented with 20% fetal calf serum (FCS), 125 mg/mL streptomycin, 125 UI/mL penicillin. At 80% of confluence, media was replaced with similar media supplemented with 15% knock-out serum (invitrogen10828-028) for 5 days to induce adipogenic differentiation (Wolins et al, 2006). Human BM-MSC were isolated from bone marrow (obtained by sternal puncture) of healthy patients as previously described (Corre et al, 2007). BM-MSC (passage 2) were seeded at $3x10^5$ cell/well in 6-well plates for 2 days in MEM alpha supplemented with 10% fetal calf serum (FCS), 125mg/mL streptomycin, 125UI/mL penicillin. At 80% of confluence, media was replaced with StemMACS™ AdipoDiff Media (Miltenyi 130-091-677) supplemented with 125mg/mL streptomycin, 125UI/mL penicillin to induce adipogenic differentiation for 28 days. Media was changed every 2 to 3 days and cells were grown in a humid atmosphere with 5% CO2 at 37°C. TG content of cells before and at the end of adipogenic differentiation was performed as previously described (Dirat et al, 2011) using commercial kit (Sigma- F6428).

Western blot

Isolated adipocytes were washed 3 times with PBS and proteins were separated from lipids using MTBE extraction described above (proteomic analysis section). Five µg of proteins were reduced with modified Laemmli buffer for 15 minutes at 65°C, loaded on 4-10% gradient SDS-PAGE gel (Biorad) and transferred to nitrocellulose membrane. Membranes were blocked with 5% skimmed milk in TBS (20mM Tris, 150mM NaCl) and incubated with appropriate primary antibodies (rabbit polyclonal antibody (pAb) anti ATGL, (1/:1000, ref: 2138, Cell Signaling Technology); rabbit pAb anti HSL (1:1000, ref: 4107, Cell Signaling Technology); rabbit pAb anti MAGL (1:1000, ref: sc134749, Santa Cruz Biotechnology); mouse monoclonal anti β-Actin (1:5000, clone: AC-15, Sigma Aldrich). The membranes were washed with TBS complemented with 0.1% Tween-20 and incubated with HRP conjugated secondary antibodies (1:5000, Santacruz Biotechnology). The immunoreactive protein bands were revealed by ECL prime Western blotting detection reagent (Ammersham™) and detected using ChemiDoc™ Imaging System (Biorad). Densitometry quantification was performed using image lab software (v5.2.1; Biorad). Signal intensity was normalized to β-Actin.

Lipolysis assay

Isolated adipocytes (50µl) were incubated with 450 µL KRBHA with or without isoprenaline 10^{-6} mol. L^{-1} (Sigma Aldrich) to evaluate stimulated and basal lipolysis respectively. After 2 h incubation at 37°C under gentle shaking, 200 µL of incubation media was removed and kept to measure glycerol and FA release using commercial kits (Sigma- F6428 and Wako diagnostic NEFA-HR, respectively). Results were normalized to total lipid content quantified after Dole extraction. Briefly, isolated adipocytes were lysed by the addition of Dole's Reagent (40:10:1 isopropanol : heptane : H_2SO_4 1N). Upper phase containing lipids was extracted again with heptane, evaporated under a nitrogen stream and dried lipids were weighted. For lipolysis experiment on adipocyte-differentiated cell lines (3T3 F442A and OP9) and human BM-MSC, cells were incubated for 3 hours and results were normalized to TG content. At the end of the incubation, cells were washed with PBS and resuspended in buffer containing 10mM Tris HCL pH 7.5 and 1mM EDTA to quantify TG.

Statistical analyses

Statistical analyses were performed using Prism v4 (GraphPad Software). Comparison between two groups was performed using paired Student's t-test and multiple comparisons was performed by two-way ANOVA follow by Bonferroni post-test for n independent experiments. P-value was considered significant if lower than 0.05.

Acknowledgements

This work benefited from the assistance of Stephanie Balor and Vanessa Soldan from the Multiscale Electron Imaging platform (METi) of the Centre de Biologie Intégrative (Toulouse, France). Lipidomic analysis was performed at the Mass Spectrometry Facility of the Beth Israel Deaconess Medical Center (Boston, USA). This work by supported by the "Fondation de France (contract N° 171352) for running costs and a two-year post-doctoral fellowship for Camille Attané. David Estève received a post-doctoral fellowship from the Fondation pour La Recherche Médicale (SPF201809007124). This work also benefited from the Toulouse Réseau Imagerie (TRI)-RIO Optical Imaging Platform at the Institute of Pharmacology and Structural Biology (Genotoul, Toulouse, France) supported by grants from the Région Midi-Pyrénées (contrat de projets état-région), the Grand Toulouse community, the Association pour la Recherche sur le Cancer (Equipement 8505), the CNRS and the European Union through the Fonds Européen de Développement Régional program. We thank Life Science Editors for editorial assistance.

Author contributions

NR set up the conditions for harvesting BM-AT and SC-AT in close collaboration with CA and DE and supervised the samples collection. CA, DE, MM handled the AT samples and isolated adipocytes. DE performed the transmission electron microscopy (with the help of the METi platform) and the immunofluorescence experiments as well as image data analysis. CA performed sample preparation for proteomic and lipidomic studies, Western blot, cell culture (with the help of MM) and the lipolysis experiments. JC performed the isolation of human BM-MSC. KC performed the proteomics studies under the supervision of OS. DE and CA conducted analysis of lipidomic (with the help of PV) and proteomic data under the supervision of JI. CA, DE, PV, OS and CM analyzed the data. CA, DE and CM conceived the idea for this project and wrote the manuscript with significant inputs from all authors. CM supervised the study.

Conflict of interest

The authors declare they have no conflict of interest

References

Abella E, Feliu E, Granada I, Milla F, Oriol A, Ribera JM, Sanchez-Planell L, Berga LI, Reverter JC, Rozman C (2002) Bone marrow changes in anorexia nervosa are correlated with the amount of weight loss and not with other clinical findings. *American Journal of Clinical Pathology* **118:** 582-588

Bartelt A, Heeren J (2014) Adipose tissue browning and metabolic health. *Nature Reviews Endocrinology* **10:** 24-36

Bathija A, Davis S, Trubowitz S (1979) Bone marrow adipose tissue: response to acute starvation. *American Journal of Hematology* **6:** 191-198

Bredella MA, Torriani M, Ghomi RH, Thomas BJ, Brick DJ, Gerweck AV, Rosen CJ, Klibanski A, Miller KK (2010) Vertebral Bone Marrow Fat Is Positively Associated With Visceral Fat and Inversely Associated With IGF-1 in Obese Women. *Obesity* **19:** 49-53

Breitkopf SB, Ricoult SJH, Yuan M, Xu Y, Peake DA, Manning BD, Asara JM (2017) A relative quantitative positive/negative ion switching method for untargeted lipidomics via high resolution LC-MS/MS from any biological source. *Metabolomics : Official Journal of the Metabolomic Society* **13**

Cawthorn William P, Scheller Erica L, Learman Brian S, Parlee Sebastian D, Simon Becky R, Mori H, Ning X, Bree Adam J, Schell B, Broome David T, Soliman Sandra S, DelProposto Jenifer L, Lumeng Carey N, Mitra A, Pandit Sandeep V, Gallagher Katherine A, Miller Joshua D, Krishnan V, Hui Susanta K, Bredella Miriam A, Fazeli Pouneh K, Klibanski A, Horowitz Mark C, Rosen Clifford J, MacDougald Ormond A (2014) Bone Marrow Adipose Tissue Is an Endocrine Organ that Contributes to Increased Circulating Adiponectin during Caloric Restriction. *Cell Metabolism* **20:** 368-375

Cawthorn WP, Scheller EL, Parlee SD, Pham HA, Learman BS, Redshaw CMH, Sulston RJ, Burr AA, Das AK, Simon BR, Mori H, Bree AJ, Schell B, Krishnan V, MacDougald OA (2016) Expansion of Bone Marrow Adipose Tissue During Caloric Restriction Is Associated With Increased Circulating Glucocorticoids and Not With Hypoleptinemia. *Endocrinology* **157:** 508-521

Cinti S (2001) The adipose organ: morphological perspectives of adipose tissues. *The Proceedings of the Nutrition Society* **60:** 319-328

Corre J, Mahtouk K, Attal M, Gadelorge M, Huynh A, Fleury-Cappellesso S, Danho C, Laharrague P, Klein B, Reme T, Bourin P (2007) Bone marrow mesenchymal stem cells are abnormal in multiple myeloma. *Leukemia* **21:** 1079-1088

Devlin MJ, Cloutier AM, Thomas NA, Panus DA, Lotinun S, Pinz I, Baron R, Rosen CJ, Bouxsein ML (2010) Caloric restriction leads to high marrow adiposity and low bone mass in growing mice. *Journal of Bone and Mineral Research* **25:** 2078-2088

Diedrich JD, Rajagurubandara E, Herroon MK, Mahapatra G, Huttemann M, Podgorski I (2016) Bone marrow adipocytes promote the Warburg phenotype in metastatic prostate tumors via HIF-1alpha activation. *Oncotarget* **7:** 64854-64877

Dirat B, Bochet L, Dabek M, Daviaud D, Dauvillier S, Majed B, Wang YY, Meulle A, Salles B, Le Gonidec S, Garrido I, Escourrou G, Valet P, Muller C (2011) Cancer-associated adipocytes exhibit an activated phenotype and contribute to breast cancer invasion. *Cancer Research* **71:** 2455-2465

Doucette CR, Horowitz MC, Berry R, MacDougald OA, Anunciado-Koza R, Koza RA, Rosen CJ (2015) A High Fat Diet Increases Bone Marrow Adipose Tissue (MAT) But Does Not Alter Trabecular or Cortical Bone Mass in C57BL/6J Mice. *Journal of Cellular Physiology* **230:** 2032-2037

Fasshauer M, Blüher M (2015) Adipokines in health and disease. *Trends in Pharmacological Sciences* **36:** 461-470

Ghali O, Al Rassy N, Hardouin P, Chauveau C (2016) Increased Bone Marrow Adiposity in a Context of Energy Deficit: The Tip of the Iceberg? *Frontiers in Endocrinology* **7**

Giordano A, Smorlesi A, Frontini A, Barbatelli G, Cinti S (2014) White, brown and pink adipocytes: the extraordinary plasticity of the adipose organ. *European journal of Endocrinology* **170:** R159-171

Hardaway AL, Herroon MK, Rajagurubandara E, Podgorski I (2015) Marrow adipocyte-derived CXCL1 and CXCL2 contribute to osteolysis in metastatic prostate cancer. *Clinical & Experimental Metastasis* **32:** 353-368

Herroon MK, Rajagurubandara E, Hardaway AL, Powell K, Turchick A, Feldmann D, Podgorski I (2013) Bone marrow adipocytes promote tumor growth in bone via FABP4-dependent mechanisms. *Oncotarget* **4:** 2108-2123

Hindorf C, Glatting G, Chiesa C, Lindén O, Flux G (2010) EANM Dosimetry Committee guidelines for bone marrow and whole-body dosimetry. *European Journal of Nuclear Medicine and Molecular Imaging* **37:** 1238-1250

Hodson L, Skeaff CM, Fielding BA (2008) Fatty acid composition of adipose tissue and blood in humans and its use as a biomarker of dietary intake. *Progress in Lipid Research* **47:** 348-380

Justesen J, Stenderup K, Ebbesen EN, Mosekilde L, Steiniche T, Kassem M (2001) Adipocyte tissue volume in bone marrow is increased with aging and in patients with osteoporosis. *Biogerontology* **2:** 165-171

Kim SH, Cho KW, Choi HS, Park SJ, Rhee Y, Jung HS, Lim SK (2009) The forkhead transcription factor Foxc2 stimulates osteoblast differentiation. *Biochemical and Biophysical Research Communications* **386:** 532-536

Krings A, Rahman S, Huang S, Lu Y, Czernik PJ, Lecka-Czernik B (2012) Bone marrow fat has brown adipose tissue characteristics, which are attenuated with aging and diabetes. *Bone* **50:** 546-552

Lafontan M, Langin D (2009) Lipolysis and lipid mobilization in human adipose tissue. *Progress in Lipid Research* **48:** 275-297

Lee MJ, Fried SK (2014) Optimal protocol for the differentiation and metabolic analysis of human adipose stromal cells. *Methods in Enzymology* **538:** 49-65

Leitner BP, Huang S, Brychta RJ, Duckworth CJ, Baskin AS, McGehee S, Tal I, Dieckmann W, Gupta G, Kolodny GM, Pacak K, Herscovitch P, Cypess AM, Chen KY (2017) Mapping of human brown adipose tissue in lean and obese young men. *Proceedings of the National Academy of Sciences of the United States of America* **114:** 8649-8654

Litvinov DY, Savushkin EV, Dergunov AD (2018) Intracellular and Plasma Membrane Events in Cholesterol Transport and Homeostasis. *Journal of Lipids* **2018:** 3965054

Liu Z, Xu J, He J, Liu H, Lin P, Wan X, Navone NM, Tong Q, Kwak LW, Orlowski RZ, Yang J (2015) Mature adipocytes in bone marrow protect myeloma cells against chemotherapy through autophagy activation. *Oncotarget* **6:** 34329-34341

Mattiucci D, Maurizi G, Izzi V, Cenci L, Ciarlantini M, Mancini S, Mensà E, Pascarella R, Vivarelli M, Olivieri A, Leoni P, Poloni A (2018) Bone marrow adipocytes support hematopoietic stem cell survival. *Journal of Cellular Physiology* **233:** 1500-1511

Meulle A, Salles B, Daviaud D, Valet P, Muller C (2008) Positive regulation of DNA double strand break repair activity during differentiation of long life span cells: the example of adipogenesis. *PLoS One* **3:** e3345

Naveiras O, Nardi V, Wenzel PL, Hauschka PV, Fahey F, Daley GQ (2009) Bone-marrow adipocytes as negative regulators of the haematopoietic microenvironment. *Nature* **460:** 259-263

Nedergaard J, Bengtsson T, Cannon B (2007) Unexpected evidence for active brown adipose tissue in adult humans. *Am J Physiol Endocrinol Metab* **293:** E444-452

Ninomiya Y, Sugahara-Yamashita Y, Nakachi Y, Tokuzawa Y, Okazaki Y, Nishiyama M (2010) Development of a rapid culture method to induce adipocyte differentiation of human bone marrow-derived mesenchymal stem cells. *Biochemical and Biophysical Research Communications* **394:** 303-308

Nishikata I, Nakahata S, Saito Y, Kaneda K, Ichihara E, Yamakawa N, Morishita K (2011) Sumoylation of MEL1S at lysine 568 and its interaction with CtBP facilitates its repressor activity and the blockade of G-CSF-induced myeloid differentiation. *Oncogene* **30:** 4194-4207

Prentice KJ, Saksi J, Hotamisligil GS (2019) Adipokine FABP4 integrates energy stores and counter regulatory metabolic responses. *Journal of Lipid Research*

Robles H, Park S, Joens MS, Fitzpatrick JAJ, Craft CS, Scheller EL (2019) Characterization of the bone marrow adipocyte niche with three-dimensional electron microscopy. *Bone* **118:** 89-98

Saito M, Okamatsu-Ogura Y, Matsushita M, Watanabe K, Yoneshiro T, Nio-Kobayashi J, Iwanaga T, Miyagawa M, Kameya T, Nakada K, Kawai Y, Tsujisaki M (2009) High incidence of metabolically active brown adipose tissue in healthy adult humans: effects of cold exposure and adiposity. *Diabetes* **58:** 1526-1531

Scheller EL, Cawthorn WP, Burr AA, Horowitz MC, MacDougald OA (2016) Marrow Adipose Tissue: Trimming the Fat. *Trends in Endocrinology and Metabolism* **27:** 392-403

Scheller EL, Doucette CR, Learman BS, Cawthorn WP, Khandaker S, Schell B, Wu B, Ding SY, Bredella MA, Fazeli PK, Khoury B, Jepsen KJ, Pilch PF, Klibanski A, Rosen CJ, MacDougald OA (2015) Region-specific variation in the properties of skeletal adipocytes reveals regulated and constitutive marrow adipose tissues. *Nature Communications* **6:** 7808

Scheller EL, Khandaker S, Learman BS, Cawthorn WP, Anderson LM, Pham HA, Robles H, Wang Z, Li Z, Parlee SD, Simon BR, Mori H, Bree AJ, Craft CS, MacDougald OA (2019) Bone marrow adipocytes resist lipolysis and remodeling in response to beta-adrenergic stimulation. *Bone* **118:** 32-41

Scheller EL, Rosen CJ (2014) What's the matter with MAT? Marrow adipose tissue, metabolism, and skeletal health. *Ann N Y Acad Sci* **1311:** 14-30

Schreibman PH, Dell RB (1975) Human adipocyte cholesterol. Concentration, localization, synthesis, and turnover. *The Journal of Clinical Investigation* **55:** 986-993

Scott MA, Nguyen VT, Levi B, James AW (2011) Current methods of adipogenic differentiation of mesenchymal stem cells. *Stem Cells and Development* **20:** 1793-1804

Shafat MS, Oellerich T, Mohr S, Robinson SD, Edwards DR, Marlein CR, Piddock RE, Fenech M, Zaitseva L, Abdul-Aziz A, Turner J, Watkins JA, Lawes M, Bowles KM, Rushworth SA (2017) Leukemic blasts program bone marrow adipocytes to generate a protumoral microenvironment. *Blood* **129:** 1320-1332

Tabe Y, Yamamoto S, Saitoh K, Sekihara K, Monma N, Ikeo K, Mogushi K, Shikami M, Ruvolo V, Ishizawa J, Hail N, Kazuno S, Igarashi M, Matsushita H, Yamanaka Y, Arai H, Nagaoka I, Miida T, Hayashizaki Y, Konopleva M, Andreeff M (2017) Bone Marrow Adipocytes Facilitate Fatty Acid Oxidation Activating AMPK and a Transcriptional Network Supporting Survival of Acute Monocytic Leukemia Cells. *Cancer Research* **77:** 1453-1464

Taschler U, Radner FP, Heier C, Schreiber R, Schweiger M, Schoiswohl G, Preiss-Landl K, Jaeger D, Reiter B, Koefeler HC, Wojciechowski J, Theussl C, Penninger JM, Lass A, Haemmerle G, Zechner R, Zimmermann R (2011) Monoglyceride lipase deficiency in mice impairs lipolysis and attenuates diet-induced insulin resistance. *The Journal of Biological Chemistry* **286:** 17467-17477

Tavassoli M (1974) Differential response of bone marrow and extramedullary adipose cells to starvation. *Experientia* **30:** 424-425

Wen PC, Mahinthichaichan P, Trebesch N, Jiang T, Zhao Z, Shinn E, Wang Y, Shekhar M, Kapoor K, Chan CK, Tajkhorshid E (2018) Microscopic view of lipids and their diverse biological functions. *Current Opinion in Structural Biology* **51:** 177-186

Wolins NE, Quaynor BK, Skinner JR, Tzekov A, Park C, Choi K, Bickel PE (2006) OP9 mouse stromal cells rapidly differentiate into adipocytes: characterization of a useful new model of adipogenesis. *Journal of Lipid Research* **47:** 450-460

Wu J, Bostrom P, Sparks LM, Ye L, Choi JH, Giang AH, Khandekar M, Virtanen KA, Nuutila P, Schaart G, Huang K, Tu H, van Marken Lichtenbelt WD, Hoeks J, Enerback S, Schrauwen P, Spiegelman BM (2012) Beige adipocytes are a distinct type of thermogenic fat cell in mouse and human. *Cell* **150:** 366-376

Yeung DKW, Griffith JF, Antonio GE, Lee FKH, Woo J, Leung PC (2005) Osteoporosis is associated with increased marrow fat content and decreased marrow fat unsaturation: A proton MR spectroscopy study. *Journal of Magnetic Resonance Imaging* **22:** 279-285

Zechner R (2015) FAT FLUX: enzymes, regulators, and pathophysiology of intracellular lipolysis. *EMBO Molecular Medicine* **7:** 359-362

Zhao S, Mugabo Y, Ballentine G, Attane C, Iglesias J, Poursharifi P, Zhang D, Nguyen Thuy A, Erb H, Prentki R, Peyot M-L, Joly E, Tobin S, Fulton S, Brown JM, Madiraju SRM, Prentki M (2016) α/β-Hydrolase Domain 6 Deletion Induces Adipose Browning and Prevents Obesity and Type 2 Diabetes. *Cell Reports* **14:** 2872-2888

Zhou BO, Yu H, Yue R, Zhao Z, Rios JJ, Naveiras O, Morrison SJ (2017) Bone marrow adipocytes promote the regeneration of stem cells and haematopoiesis by secreting SCF. *Nature Cell Biology* **19:** 891-903

Zingaretti MC, Crosta F, Vitali A, Guerrieri M, Frontini A, Cannon B, Nedergaard J, Cinti S (2009) The presence of UCP1 demonstrates that metabolically active adipose tissue in the neck of adult humans truly represents brown adipose tissue. *FASEB J* **23:** 3113-3120

Zwick RK, Guerrero-Juarez CF, Horsley V, Plikus MV (2018) Anatomical, Physiological, and Functional Diversity of Adipose Tissue. *Cell Metabolism* **27:** 68-83

Figure legends

Fig 1: SC-Ad and BM-Ad exhibit similar morphological properties.

A. Scheme of the experimental protocol designed to obtain paired human primary bone marrow (BM-Ad) and subcutaneous adipocytes (SC-Ad). Paired bone marrow (BM-AT) and subcutaneous adipose tissues (SC-AT) were harvested from patients undergoing hip replacement surgery. BM-AT, that share the same macroscopic aspects compared to SC-AT, was isolated from the red bone marrow containing hematopoietic cells. After enzymatic digestion, floating cells were rinsed and collected for subsequent experiments.

B. Whole mount SC-AT and BM-AT were stained with Bodipy 493/503 (neutral lipids, green), Phalloidin (F-Actin, red) and TOPRO-3 (nucleus, blue). Z stack images were taken using confocal microscope with 10X objective (n=3). Representative maximum intensity projection is shown. Orange arrowheads show vessels. White arrowheads show stromal cells. Scale bar, 100µm.

C. Transmission electron microscopy images of SC-AT and BM-AT. N: Nucleus, LD: Lipid Droplet, C: cytoplasm. Scale bar, 0.5µm.

D. Primary SC-Ad and BM-Ad were isolated and stained with Bodipy 493/503 (neutral lipids, green), phalloidin (F-actin, red) and TOPRO3 (nucleus, blue). Z stack images were taken using confocal microscope with 40X objective (n=3). Representative maximum intensity projection is shown. Scale bar, 50µm.

Fig 2: Detailed lipid species analysis of BM-Ad shows increase free cholesterol and MG contents compared to SC-Ad.

A. Total lipid content in SC-AT and BM-AT (left, n=7) and in SC-Ad and BM-Ad (right, n=17) were extracted and weighted. The quantity of lipids was normalized to the quantity of tissue or the volume of adipocyte from which lipids were extracted. Histograms represent mean ± SEM. ns stands for non-significant according to paired t test.

B. Pie chart of the relative abundance of the detected lipid classes using large-scale LC-MS/MS approaches. The glycerolipids (GL) are shown in blue shades. TG: triacylglycerol, DG: diacylglycerol, MG: monoacylglycerol; Phospholipids (PL) are in green shades. PC: phosphatidylcholine, PE: Phosphatidylethanolamine, PG: phosphatidylglycerol, PI: Phostatidylinositol, PS: Phosphatidylserine, LPC: Lysophosphatidylcholine, LPE: Lysophosphatidylethanolamine, Sphingolipids (SL) are in yellow shades. SM: Sphingomyeline, Cer: Ceramides, So: Sphingosine; and fatty acid esters (FAE) are in pink shades. WE: Wax Ester, AcCA: Acyl Carnitine.

C. Violin plot representing the log2 fold change of the 15 lipid classes identified in BM-Ad compared to SC-Ad analyzed by LC-MS/MS (n= 4). The quantity of lipid classes were calculated as the sum of the different lipid species belonging to the same classes.

D: Free cholesterol contents were measured using an enzymatic assay on lipid extracted from BM-Ad and SC-Ad. The results were normalized to the quantity of total lipids. The histograms represent mean ± SEM, *** p<0. 001 according to paired t test (n= 11).

Fig 3: Large-scale proteome analysis highlights differences in lipid metabolism between BM-Ad and SC-Ad.

A. Principal component analysis of BM-Ad (grey) and SC-Ad (black) based on the relative quantification of the abundance of the proteins involved in lipid and glucose metabolism identified in the LC-MS/MS dataset. The first two components and the percentage of variance for each component are shown. Ellipses show the 95% confidence are interval to strengthen the clustering of the tissues according to their anatomical locations.

B. Volcano plot of the 612 proteins involved in lipid and glucose metabolism identified and quantified using LC-MS/MS analysis. Sixty seven proteins are significantly ($p < 0.05$) enriched in BM-Ad (red circles), whereas 68 proteins are significantly ($p < 0.05$) down-regulated (blue circle) and 477 are unmodified (open circle) in BM-Ad compared to SC-Ad according to linear model statistical analysis.

C. Pathway enrichment analysis performed with gene analytics. The top pathways enriched in BM-Ad (red bars) and down-regulated (blue bars) are presented.

D. Heatmap of the relative abundance of proteins differentially expressed in BM-Ad and SC-Ad belonging to the lipoprotein metabolism pathway. Dendrogram represents hierarchical clustering of the samples. Blue squares represent down regulated proteins and red squares enriched proteins.

Fig 4: Human native BM-Ad are devoid of lipolytic activity, a metabolic trait not recapitulated by primary BM-MSCs differentiated *in vitro*.

A. Left panel: Western blot analyses of the three main enzymes involved in lipolysis on paired isolated SC-Ad (SC) and BM-Ad (M) from 3 independent donors. β-actin is shown as loading control. Right panel: relative quantifications of the band intensity normalized to the quantity of β-actin. The histograms represent mean ± SEM. ns=not significant. ** $p<0.01$ according to paired Student's t-test.

B. Glycerol release was measured from isolated SC-Ad and BM-Ad as readout of complete lipolysis under basal condition (plain bar) or after stimulation with isoprenaline (hatched bar). The data are mean of 7 independent experiments and normalized to the quantity of the total lipids content. The histograms represent mean ± SEM, ns, not significant; ***$p<0.001$ according to two-way ANOVA followed by Bonferroni post-test.

C. Free fatty acids (FFA) release from isolated SC-Ad and BM-Ad as readout of lipolysis under basal condition (plain bar) or after stimulation with isoprenaline (hatched bar). Data are mean of 7 independent experiments and are normalized to the quantity of the total lipids content. The histograms represent mean ± SEM, ns, not significant; **$p<0.01$ according to two-way ANOVA followed by Bonferroni post-test.

D. TG content was measured in cell lysates from 3T3F442A (3T3) and OP9 cell lines or human BM-MSC (MSC) before and after adipogenic differentiation (nd: non-differentiated, d: differentiated). Data are mean of at least 4 independent experiments (4 independent donors were used for human BM-MSC) and were normalized to the quantity of the total protein content. The histograms represent mean ± SEM, *$p<0.05$; **$p<0.01$according to two-way ANOVA followed by Bonferroni post-test

E. Glycerol release from *in vitro* differentiated 3T3F442A (3T3) and OP9 cell lines or human BM-MSC (MSC) as readout of complete lipolysis under basal conditions (plain bar) or after stimulation with isoprenaline (hatched bar). The data are mean of 3 independent experiments (3 independent donors were used for human BM-MSC) and were normalized to the quantity of the total lipids content. The histograms represent mean ± SEM, * $p<0.05$; **$p<0.01$ according to two-way ANOVA followed by Bonferroni post-test.

Expanded View Figure legends

Fig EV1: SC-Ad and BM-Ad exhibit similar morphology

A. Whole mount SC-AT and BM-AT were stained with an antibody directed against perilipin 1 (PLIN1, green), phalloidin (F-Actin, red) and TOPRO-3 (nucleus, blue). Z stack images were taken using confocal microscope with 40X objective (n=3). Representative maximum intensity projection is shown. Orange arrowheads show vessels and white arrowheads show stromal cells. Scale bar=50µm.

B. Representative XY and YZ focal planes are shown to highlight the cohesive organization of the SC- and BM-AT and the thin cytoplasm of adipocytes (blue arrowheads).

Fig EV2: Unsupervised lipidomic analyses reveal that the variance between samples mainly occur through inter-individual variability despite increased MG species in BM-Ad.

A. Principal component analysis of BM-Ad (grey) and SC-Ad (black) based on the relative quantification of the lipid species identified in LC-MS/MS. The first two components and the percentage of variance for each component are shown.

B. Heatmap of the relative abundance of lipid species quantified in BM-Ad and SC-Ad. Dendrogram represents hierarchical clustering of samples. Blue squares represent down-regulated lipid species and red squares enriched lipid species.

C. Relative quantification of the main MG species by LC-MS/MS in paired isolated SC-Ad and BM-Ad (n= 4). Histograms represent mean ± SEM, * $p<0.05$ according to two way ANOVA followed by Bonferroni's post-test.

Fig EV3. Large-scale analysis of the proteome reveals differences in lipid metabolism, but not adipokines, between BM-Ad and SC-Ad.

A. Scheme of the proteomic dataset analysis workflow. Extracted proteins from paired isolated SC- and BM-Ad were analyzed by LC-MS/MS. Among the 3787 proteins identified, 3259 were robustly identified in at least 3 of 4 donors. We selected a set of 612 proteins involved in lipid and glucose metabolism using gene analytics software to perform the statistical and bioinformatics analyses. In this dataset, unsupervised multivariate analysis was performed and differentially expressed proteins were identified using a linear statistical model (LIMMA) allowing to identify 67 proteins enriched and 68 proteins downregulated in BM-Ad compared to SC-Ad. Pathway enrichment analyses were performed using gene analytics software that concatenates several databases to identify specific lipid pathways enriched and down regulated in BM-Ad. Hierarchical clustering analyses were then performed on these specific lipid pathways.

B. Heatmap of the relative abundance of adipokines expressed in BM-Ad and SC-Ad. Dendrogram represents hierarchical clustering of the samples. Blue squares represents down regulated proteins and red squares enriched proteins.

C. Heatmaps of the relative abundance of proteins differentially expressed in BM-Ad and SC-Ad belonging to the Cholesterol Biosynthesis I and Statin pathway. Dendrogram represents hierarchical clustering of the samples. Blue squares represent down regulated proteins and red squares enriched proteins.

D. Heatmap of the relative abundance of proteins differentially expressed in BM-Ad and SC-Ad belonging to the arachidonic acid metabolism pathway. Dendrogram represents hierarchical clustering of the samples. Blue squares represents down regulated proteins and red squares enriched proteins.

E. Heatmap of the relative abundance of proteins differentially expressed in BM-Ad and SC-Ad belonging to the FA metabolism pathway. Dendrogram represents hierarchical clustering of the samples. Blue squares represent down regulated proteins. Red squares enriched proteins.

Supplementary Table 1:

Protein expression involved in lipid and glucose metabolism were quantified by nano LC-MS/MS. The log2 transformed average intensities of label free quantification (LFQ) in BM-Ad and SC-Ad for each protein in the dataset and the corresponding log2 fold change and p-Value are presented.

Gene Symbol	Average expression in BM-Ad (log2 LFQ intensity)	Average expression in SC-Ad (log2 LFQ intensity)	log2 Fold change (BM-Ad / SC-Ad)	P.Value
S100A4	21,510	28,158	-6,647	7,512E-05
PPP1R1B	19,924	24,015	-4,091	1,321E-05
CLPP	20,921	24,880	-3,959	4,754E-03
ALDH1A1	24,112	27,738	-3,625	8,082E-02
ALDOC	25,733	29,330	-3,598	4,918E-05
SORBS1	23,500	26,875	-3,375	5,411E-03
PEMT	19,394	22,593	-3,199	6,775E-03
PHGDH	24,128	27,283	-3,155	2,538E-02
VLDLR	20,088	23,180	-3,092	6,984E-03
CSNK1G1	19,433	22,478	-3,044	1,903E-05
EIF4B	21,238	24,183	-2,945	1,053E-03
PTPRF	22,233	25,150	-2,917	2,989E-02
SH3KBP1	24,630	27,425	-2,795	2,680E-03
S100A6	26,210	28,958	-2,748	1,790E-03
ACSS2	22,832	25,485	-2,653	4,720E-02
EIF4H	22,319	24,938	-2,618	1,063E-02
UAP1	21,296	23,913	-2,617	1,852E-02
PTGR2	21,648	24,170	-2,522	8,235E-03
TXN2	21,132	23,585	-2,453	2,475E-02
MGLL	29,233	31,678	-2,445	2,382E-04
RAB9A	23,678	25,995	-2,318	1,546E-03
MAP2K2	21,165	23,458	-2,292	9,283E-03
ME3	22,294	24,573	-2,279	1,045E-01
SYNJ1	20,786	23,012	-2,226	1,832E-01
ACAD11	22,650	24,873	-2,223	8,743E-02
PLIN3	25,140	27,360	-2,220	5,936E-02
ACBD5	21,051	23,270	-2,219	6,033E-02
ACOT2	22,473	24,650	-2,177	1,240E-01

EXOC7	20,732	22,880	-2,148	2,903E-02
ADH1C	27,700	29,848	-2,148	4,060E-02
S100B	24,340	26,405	-2,065	1,691E-02
BDH1	21,644	23,685	-2,041	4,369E-02
ENPP1	24,585	26,575	-1,990	3,336E-02
MDH1	29,085	31,038	-1,953	4,880E-03
AKR1C2	28,260	30,180	-1,920	1,803E-03
COPZ2	21,636	23,480	-1,844	2,309E-02
ACADSB	24,280	26,115	-1,835	1,092E-02
GCDH	23,505	25,298	-1,793	7,491E-02
EPHX2	20,757	22,510	-1,753	5,034E-02
NQO1	28,498	30,248	-1,750	1,928E-02
PTGIS	21,603	23,333	-1,729	1,778E-01
PIK3R1	20,423	22,140	-1,717	2,594E-02
MRAS	25,950	27,653	-1,703	3,280E-03
AKAP1	21,940	23,623	-1,683	1,381E-02
MCEE	22,652	24,313	-1,661	8,804E-02
TOMM20	21,184	22,798	-1,614	3,009E-02
PLIN1	34,325	35,935	-1,610	1,040E-02
PCYT2	22,651	24,243	-1,592	1,259E-01
RELA	25,958	27,548	-1,590	7,966E-03
DDHD2	20,702	22,280	-1,578	3,466E-02
ACAT1	29,143	30,708	-1,565	6,936E-03
ANXA1	31,820	33,375	-1,555	9,500E-03
CBR3	23,495	25,018	-1,523	5,170E-02
GBE1	27,890	29,398	-1,508	1,802E-02
PRDX6	30,043	31,543	-1,500	2,034E-02
PYGB	26,510	27,990	-1,480	6,462E-02
TNFAIP8	21,773	23,248	-1,475	5,419E-02
AKR1C3	27,375	28,843	-1,467	1,787E-02
ARSA	21,528	22,990	-1,463	3,140E-02
GNPDA2	20,600	22,058	-1,457	3,903E-02
TKT	30,495	31,950	-1,455	1,336E-02
ACAD9	28,818	30,255	-1,438	1,406E-01
PDE3B	21,590	23,023	-1,433	8,953E-02
EIF2B3	19,956	21,368	-1,411	1,522E-01
CLTA	23,173	24,578	-1,405	1,231E-01
ANXA5	31,740	33,143	-1,403	9,549E-03
THRAP3	20,393	21,785	-1,392	1,437E-02
ME1	25,840	27,218	-1,378	1,086E-01
HK2	22,870	24,243	-1,373	2,638E-01
DECR2	23,328	24,683	-1,355	1,035E-01
CRAT	25,320	26,658	-1,338	4,616E-02
MPI	22,198	23,528	-1,329	1,210E-01
PRKCD	23,428	24,748	-1,320	2,517E-02

SAR1B	24,960	26,275	-1,315	1,314E-02
IDH3B	26,545	27,840	-1,295	2,022E-02
GRB2	23,590	24,885	-1,295	3,304E-01
EIF2S2	26,633	27,925	-1,292	3,025E-02
CRKL	22,267	23,553	-1,286	2,396E-01
ORMDL3	23,025	24,305	-1,280	4,234E-02
LDHA	29,758	31,033	-1,275	5,285E-02
VAPB	25,860	27,130	-1,270	1,858E-02
DBI	23,720	24,985	-1,265	1,730E-01
PDK1	21,443	22,700	-1,257	2,004E-01
GYS1	22,526	23,778	-1,252	3,687E-01
CNTFR	26,045	27,293	-1,248	6,133E-02
G6PD	27,770	27,668	-1,247	2,904E-01
PGM1	28,595	29,838	-1,243	7,183E-02
GPD1	31,363	32,605	-1,242	5,701E-02
HMOX2	24,040	25,280	-1,240	1,002E-02
ACYP2	21,996	23,233	-1,237	1,044E-01
HADH	30,430	31,653	-1,223	2,698E-02
DECR1	28,855	30,075	-1,220	1,758E-02
COPE	23,085	24,305	-1,220	1,425E-01
ALG11	21,844	23,055	-1,211	2,749E-01
FABP4	32,935	34,143	-1,208	2,608E-02
EIF4G2	22,870	24,078	-1,208	1,477E-01
SDHC	23,440	24,640	-1,200	1,993E-01
VAMP2	21,287	22,480	-1,193	3,004E-01
LIPE	30,383	31,570	-1,188	1,674E-02
NUDT14	20,362	21,544	-1,183	2,165E-01
LDHB	30,063	31,238	-1,175	2,967E-02
ELOVL5	23,850	25,008	-1,158	3,533E-02
ADH5	27,823	28,978	-1,155	3,581E-02
AGL	21,200	22,353	-1,153	3,662E-01
CALU	20,402	21,546	-1,143	4,410E-01
AGPAT3	23,693	24,803	-1,110	1,558E-01
ALDOA	30,130	31,230	-1,100	4,271E-02
ECHS1	29,710	30,810	-1,100	4,715E-02
PYGL	29,710	30,798	-1,088	6,288E-02
LMNA	32,478	32,663	-1,085	7,168E-02
MTAP	23,511	24,595	-1,084	1,741E-01
FITM2	23,398	24,478	-1,080	5,798E-02
PCBP2	25,328	25,410	-1,079	2,997E-01
STAT5A	25,683	26,758	-1,075	1,823E-01
SHMT1	24,575	25,645	-1,070	1,526E-01
RRAS2	26,798	27,858	-1,060	1,652E-02
ENO1	31,025	32,075	-1,050	7,524E-02
UGP2	30,373	31,420	-1,048	5,928E-02

COL4A3BP	21,720	22,760	-1,040	1,652E-01
JAK1	20,344	21,375	-1,031	1,251E-01
SCD	26,323	27,353	-1,030	2,444E-01
CAV1	27,958	27,965	-1,025	6,888E-02
ADH1B	31,945	32,968	-1,022	6,785E-02
GMPPB	20,315	21,326	-1,011	4,475E-01
AKT2	23,548	24,558	-1,010	5,896E-02
MYH7	22,304	23,298	-0,994	6,288E-01
PEA15	24,450	25,443	-0,992	5,581E-02
STAT5B	22,183	23,173	-0,989	2,915E-01
ACACA	24,598	25,578	-0,980	4,458E-01
MAPK3	24,765	25,743	-0,978	1,467E-01
PTPN11	24,473	25,448	-0,975	1,107E-01
TPT1	25,693	26,668	-0,975	1,353E-01
GRHPR	26,143	27,115	-0,973	7,497E-02
ECI2	23,563	24,523	-0,960	6,278E-02
RGN	21,100	22,058	-0,958	2,620E-01
ALDH2	31,980	32,935	-0,955	8,121E-02
PPP1CC	21,130	22,080	-0,950	2,207E-01
MECR	23,565	24,510	-0,945	9,104E-02
SLC25A10	24,358	25,300	-0,942	8,690E-02
OXCT1	28,070	29,008	-0,938	6,051E-02
LNPEP	26,973	27,903	-0,930	1,339E-01
SOD2	29,673	30,603	-0,930	8,928E-02
G0S2	21,776	22,705	-0,929	2,520E-01
HAGH	24,130	25,048	-0,918	5,911E-02
MUT	25,018	25,935	-0,917	1,801E-01
ANXA2	34,183	35,095	-0,912	2,814E-02
CRK	25,943	26,845	-0,903	1,054E-01
RAB5A	25,315	26,213	-0,897	4,840E-02
ACO1	29,453	30,335	-0,883	1,360E-01
ACAA1	25,528	26,403	-0,875	7,343E-02
IDH3A	26,998	27,873	-0,875	7,145E-02
GAPDH	30,563	31,435	-0,873	5,790E-02
CAMK1	22,318	23,185	-0,868	1,827E-01
RHOA	27,368	28,233	-0,865	6,350E-02
EIF4G1	24,173	25,035	-0,863	2,585E-01
EIF2S3	25,833	26,693	-0,860	1,664E-01
THRSP	20,503	21,363	-0,859	1,567E-01
EIF4E	22,545	23,403	-0,858	3,308E-01
NFKB1	21,205	22,063	-0,858	2,634E-01
PPIA	30,053	30,910	-0,857	1,421E-01
FASN	30,600	31,458	-0,857	2,883E-01
HADHB	30,380	31,233	-0,852	5,646E-02
PECR	27,355	28,208	-0,852	6,796E-02

MIF	23,883	24,728	-0,845	2,918E-01
TSPO	27,083	27,928	-0,845	1,132E-01
ACADS	28,128	28,960	-0,833	7,945E-02
GPI	25,183	26,010	-0,827	1,741E-01
ALDH1B1	25,643	26,465	-0,823	1,673E-01
RRAS	29,753	30,575	-0,823	7,384E-02
PPP2CA	24,073	24,893	-0,820	2,076E-01
ACOT1	29,290	30,103	-0,813	1,188E-01
PGD	29,210	30,023	-0,813	1,356E-01
PGK1	29,808	30,615	-0,808	1,586E-01
CS	30,343	31,145	-0,802	1,349E-01
MMAA	20,523	21,308	-0,785	1,558E-01
ALDH3A2	29,280	30,060	-0,780	6,119E-02
KRAS	25,825	26,600	-0,775	1,303E-01
CALM3	28,003	28,773	-0,770	1,549E-01
EIF2S1	25,945	26,710	-0,765	1,644E-01
LDHD	22,758	23,523	-0,765	3,230E-01
PCCA	26,190	26,955	-0,765	3,906E-01
GPD1L	22,261	23,021	-0,760	6,414E-01
EIF4A2	25,080	25,833	-0,752	3,458E-01
GPX4	27,275	28,020	-0,745	1,683E-01
PPP1CB	25,200	25,943	-0,742	1,579E-01
PDHX	25,648	26,388	-0,740	1,683E-01
LMF1	21,719	22,458	-0,738	4,513E-01
PPP2R2A	24,848	25,585	-0,738	3,263E-01
SUCLG1	27,448	28,178	-0,730	1,321E-01
VAPA	26,855	27,568	-0,712	9,879E-02
ABCC1	19,646	20,353	-0,707	9,581E-02
FH	28,843	29,548	-0,705	9,951E-02
PRKAG1	23,095	23,800	-0,705	4,227E-01
CAT	31,095	31,798	-0,703	1,287E-01
SEC24A	19,860	20,562	-0,701	2,690E-01
LPIN1	21,059	21,758	-0,699	2,660E-01
NCL	27,858	28,545	-0,688	2,326E-01
CALU	28,695	29,378	-0,682	1,644E-01
PGLS	25,130	25,805	-0,675	3,468E-01
GLB1	21,619	22,285	-0,666	3,993E-01
PYGM	21,294	21,960	-0,666	3,060E-01
TALDO1	28,683	29,348	-0,665	1,908E-01
ACAA2	30,213	30,878	-0,665	1,494E-01
AKR1B1	24,163	24,825	-0,662	6,971E-01
BCAT2	24,810	25,470	-0,660	2,511E-01
CYCS	26,935	27,588	-0,652	1,608E-01
HMGCL	25,485	26,135	-0,650	2,553E-01
ACOT13	26,553	27,200	-0,648	1,992E-01

CLIC4	24,415	25,060	-0,645	5,769E-01
CBR1	26,430	27,073	-0,642	2,177E-01
SUCLG2	28,205	28,843	-0,637	1,526E-01
C1QBP	26,195	26,825	-0,630	1,668E-01
PRKAR2B	28,915	29,545	-0,630	2,234E-01
AP2A1	25,335	25,958	-0,622	6,271E-01
DLST	29,028	29,648	-0,620	1,610E-01
PCCB	26,420	27,030	-0,610	3,193E-01
ILK	28,618	29,225	-0,608	2,996E-01
EGFR	24,615	25,223	-0,608	2,175E-01
AKT1	20,992	21,595	-0,603	4,504E-01
MDH2	29,795	30,395	-0,600	1,701E-01
DERA	22,394	22,983	-0,589	5,086E-01
GFPT1	23,475	24,060	-0,585	5,159E-01
NANS	22,890	23,468	-0,578	5,148E-01
GLTP	22,315	22,888	-0,573	2,293E-01
CTBP1	22,645	23,215	-0,570	4,174E-01
ATP2B4	28,193	28,760	-0,568	3,037E-01
FKBP4	21,975	22,535	-0,560	6,602E-01
EIF2AK2	21,151	21,710	-0,559	3,927E-01
TNFAIP8L2	20,415	20,968	-0,553	3,841E-01
DLD	29,223	29,775	-0,553	2,426E-01
MAPK14	21,572	22,123	-0,551	4,852E-01
PDHB	28,255	28,798	-0,543	2,621E-01
RAB7A	29,295	29,838	-0,543	1,909E-01
ABHD5	27,765	28,308	-0,543	2,076E-01
SUCLA2	27,880	28,408	-0,527	2,437E-01
RAB14	29,135	29,658	-0,523	3,036E-01
CD36	33,253	33,753	-0,500	3,204E-01
CIDEC	21,030	21,530	-0,500	3,684E-01
IDH3G	25,705	26,203	-0,498	2,559E-01
AGPAT2	26,430	26,928	-0,497	3,141E-01
RAP1B	25,225	25,718	-0,493	2,454E-01
GMPPA	22,403	22,895	-0,492	4,502E-01
ACACB	27,430	27,920	-0,490	5,297E-01
PGAM1	28,978	29,465	-0,488	3,592E-01
GNA12	21,925	22,413	-0,487	3,618E-01
BCL2	24,588	25,068	-0,480	3,976E-01
GLUD1	29,300	29,780	-0,480	2,506E-01
PPP3CB	23,345	23,813	-0,467	4,656E-01
ALDH9A1	28,690	29,150	-0,460	4,400E-01
LTA4H	24,930	25,388	-0,458	6,721E-01
NSDHL	24,625	25,083	-0,457	3,236E-01
MPC2	26,690	27,145	-0,455	3,426E-01
CSNK2A2	24,240	24,693	-0,453	3,498E-01

PAFAH1B1	26,225	26,668	-0,442	3,707E-01
ALG5	24,298	24,740	-0,442	2,392E-01
RPS6	24,880	25,318	-0,438	2,872E-01
PAFAH1B2	24,738	25,165	-0,427	4,904E-01
PPID	20,817	21,243	-0,425	3,819E-01
SORT1	25,568	25,988	-0,420	3,812E-01
RAP1A	29,748	30,163	-0,415	3,081E-01
CTSD	29,870	30,270	-0,400	3,224E-01
SLC27A4	21,114	21,505	-0,391	5,333E-01
RHEB	24,123	24,513	-0,390	3,684E-01
LONP1	26,935	27,320	-0,385	4,389E-01
CTSA	23,572	23,955	-0,383	6,431E-01
ACADL	23,235	23,618	-0,383	8,034E-01
ACOX2	21,435	21,815	-0,380	5,367E-01
HSD11B1	23,778	24,155	-0,378	5,095E-01
OGDH	28,125	28,498	-0,372	6,288E-01
TPI1	29,525	29,893	-0,368	5,097E-01
TXNRD1	22,601	22,968	-0,367	7,535E-01
SRC	20,872	21,230	-0,358	6,435E-01
RHOT2	21,113	21,462	-0,349	6,649E-01
HADHA	30,450	30,795	-0,345	5,498E-01
PCYT1A	25,275	25,620	-0,345	4,611E-01
AHCYL1	24,998	25,338	-0,340	5,631E-01
HDLBP	23,980	24,320	-0,340	6,089E-01
NDUFAB1	25,295	25,635	-0,340	5,419E-01
LRPAP1	27,390	27,720	-0,330	5,653E-01
ORMDL2	24,585	24,915	-0,330	4,546E-01
ACSL1	31,823	32,150	-0,327	5,661E-01
PPP2R5A	24,455	24,780	-0,325	4,577E-01
PLA2G4A	22,945	23,265	-0,320	7,038E-01
ARCN1	25,655	25,973	-0,317	5,261E-01
GPX1	27,760	28,073	-0,313	6,313E-01
PPP2R1A	26,995	27,305	-0,310	6,006E-01
ACADVL	30,198	30,503	-0,305	4,925E-01
GLO1	25,355	25,660	-0,305	6,636E-01
AGK	23,355	23,658	-0,302	6,816E-01
PDHA1	28,103	28,393	-0,290	5,719E-01
SLC25A1	28,795	29,083	-0,288	5,751E-01
ACOT9	26,268	26,555	-0,287	5,447E-01
RAC1	21,598	21,876	-0,278	8,000E-01
ACSF2	26,685	26,963	-0,278	7,720E-01
ARF1	28,873	29,143	-0,270	6,100E-01
ACOX1	26,630	26,893	-0,262	4,995E-01
MBNL1	21,482	21,740	-0,258	5,905E-01
ACADM	28,645	28,903	-0,258	6,378E-01

CAB39	24,205	24,460	-0,255	6,102E-01
DMGDH	21,395	21,650	-0,255	6,445E-01
PPP2R5D	22,313	22,563	-0,250	6,735E-01
PRDX1	29,515	29,765	-0,250	6,517E-01
ECI1	26,585	26,830	-0,245	6,288E-01
PRDX2	29,950	30,183	-0,232	6,284E-01
ALDH7A1	27,715	27,943	-0,228	5,909E-01
PRKAR2A	27,025	27,253	-0,228	6,446E-01
TXNRD2	22,968	23,195	-0,228	7,202E-01
CBR4	22,803	23,030	-0,227	6,718E-01
MAP2K1	26,143	26,365	-0,222	6,870E-01
PRPS1	23,850	24,070	-0,220	6,957E-01
FABP5	28,043	28,260	-0,217	7,938E-01
PRKACB	25,698	25,913	-0,215	6,845E-01
PTGES2	26,315	26,530	-0,215	6,258E-01
SIRT3	22,273	22,485	-0,212	6,180E-01
RPS27A	30,510	30,723	-0,212	6,403E-01
CPNE1	22,830	23,035	-0,205	8,130E-01
EIF4A1	28,038	28,240	-0,202	7,332E-01
ACOX3	20,660	20,855	-0,195	7,095E-01
AKR1A1	26,888	27,080	-0,193	7,680E-01
OPA1	26,870	27,063	-0,193	7,149E-01
SDHA	28,620	28,808	-0,188	7,559E-01
EHHADH	25,390	25,578	-0,188	7,765E-01
LMNA	26,265	27,350	-0,185	6,737E-01
HSD17B8	23,960	24,143	-0,183	7,032E-01
SUMF1	22,393	22,573	-0,180	7,087E-01
SLC2A4	24,963	25,143	-0,180	6,969E-01
EIF2B4	20,996	21,172	-0,176	7,822E-01
MAPK10	20,077	20,248	-0,170	8,462E-01
SDHB	27,208	27,365	-0,157	7,565E-01
COPZ1	23,603	23,753	-0,150	7,910E-01
STAT6	22,450	22,600	-0,150	8,634E-01
DLAT	28,483	28,630	-0,148	7,965E-01
HSD17B4	28,750	28,888	-0,137	7,051E-01
PKM	29,508	29,640	-0,133	8,448E-01
ITGB1	31,088	31,208	-0,120	8,006E-01
PGRMC1	28,945	29,060	-0,115	8,409E-01
PTPN1	22,534	22,648	-0,113	7,828E-01
ACO2	29,810	29,920	-0,110	8,446E-01
KPNB1	26,980	27,090	-0,110	8,399E-01
MFN2	23,533	23,643	-0,110	8,982E-01
PTGES3	23,418	23,528	-0,110	8,705E-01
ABHD6	20,067	20,166	-0,099	8,263E-01
ASAH1	28,788	28,880	-0,093	8,383E-01

TM7SF2	24,763	24,855	-0,093	8,803E-01
FDPS	24,825	24,913	-0,087	9,123E-01
PCBP2	20,363	21,441	-0,082	8,716E-01
TBC1D4	19,569	19,650	-0,081	9,150E-01
PIK3C3	20,449	20,529	-0,080	9,225E-01
ACSS3	26,318	26,395	-0,078	8,845E-01
INPP5K	22,288	22,363	-0,075	8,497E-01
SEC23A	25,588	25,663	-0,075	9,066E-01
CES1	33,438	33,500	-0,062	9,284E-01
TXN	26,313	26,373	-0,060	9,126E-01
SCP2	27,105	27,165	-0,060	8,954E-01
PMVK	21,574	21,634	-0,059	9,446E-01
GNAI1	27,903	27,953	-0,050	9,270E-01
VDAC1	30,060	30,105	-0,045	9,123E-01
STAT3	25,490	25,535	-0,045	9,584E-01
ADIPOQ	26,768	26,805	-0,038	9,395E-01
ROCK1	21,362	21,395	-0,033	9,768E-01
DGAT1	25,108	25,140	-0,032	9,518E-01
MPC1	24,775	24,798	-0,023	9,599E-01
S100A1	21,333	21,353	-0,021	9,871E-01
PON2	27,218	27,233	-0,015	9,747E-01
CAV1	33,368	34,393	-0,008	9,938E-01
TPM1	23,975	23,980	-0,005	9,921E-01
NCOA2	23,270	23,270	0,000	1,000E+00
AP2A2	25,518	25,515	0,003	9,979E-01
SLC25A11	28,483	28,480	0,003	9,954E-01
VAC14	23,808	23,798	0,010	9,874E-01
PC	30,178	30,168	0,010	9,847E-01
PLBD1	22,825	22,810	0,015	9,824E-01
COPG1	24,720	24,700	0,020	9,788E-01
AP2B1	26,913	26,868	0,045	9,329E-01
RUFY1	21,838	21,780	0,058	9,355E-01
PTPMT1	22,998	22,938	0,060	9,036E-01
IL6ST	21,391	21,321	0,070	9,235E-01
LDLRAP1	19,544	19,470	0,074	8,895E-01
CPT2	26,068	25,993	0,075	8,980E-01
SLC25A5	28,065	27,973	0,092	8,147E-01
MAPK1	26,530	26,438	0,093	8,775E-01
PNPLA2	25,950	25,853	0,097	8,294E-01
RAN	27,415	27,315	0,100	8,537E-01
G6PD	23,448	24,695	0,103	8,594E-01
HSPA5	31,928	31,818	0,110	8,099E-01
PNPLA8	20,399	20,288	0,111	8,170E-01
PCK1	25,128	25,015	0,113	8,337E-01
MCU	24,275	24,160	0,115	8,109E-01

IGF2R	22,825	22,703	0,123	7,513E-01
PGM3	24,003	23,873	0,130	7,376E-01
NPC2	22,299	22,165	0,134	8,323E-01
COX4I1	30,003	29,858	0,145	7,614E-01
VDAC2	29,335	29,183	0,153	7,197E-01
SIRT5	21,632	21,463	0,169	6,768E-01
ESYT2	28,400	28,228	0,172	7,127E-01
HSD17B12	29,238	29,063	0,175	6,932E-01
WFS1	25,410	25,230	0,180	7,388E-01
ANXA7	27,615	27,425	0,190	6,878E-01
ACAT2	23,025	22,827	0,198	8,506E-01
PRKACA	29,903	29,703	0,200	6,638E-01
DHCR7	24,095	23,890	0,205	6,676E-01
CDC42	27,693	27,483	0,210	5,829E-01
RHOQ	22,440	22,228	0,213	6,985E-01
P4HB	32,263	32,050	0,213	6,262E-01
CARM1	21,909	21,678	0,232	7,195E-01
YAP1	23,905	23,663	0,242	6,723E-01
H6PD	27,663	27,420	0,243	5,989E-01
SLC9A3R2	22,978	22,733	0,245	5,944E-01
PRKAA1	23,493	23,245	0,248	6,717E-01
PHKB	20,700	20,450	0,249	7,253E-01
LPGAT1	25,248	24,983	0,265	6,057E-01
CPNE3	26,935	26,668	0,268	5,423E-01
UGP2	22,192	21,924	0,268	8,071E-01
IDH1	31,438	31,165	0,272	6,725E-01
HK1	26,990	26,715	0,275	5,704E-01
LEP	23,165	22,888	0,277	8,457E-01
PRKAR1A	24,745	24,465	0,280	5,971E-01
COPB2	25,823	25,540	0,282	7,023E-01
OSBP	23,355	23,068	0,287	6,015E-01
RAC3	22,150	21,858	0,292	7,934E-01
EEF2	28,585	28,290	0,295	5,880E-01
CSNK2B	24,240	23,943	0,297	4,811E-01
BID	20,617	20,305	0,312	4,774E-01
RAC1	28,920	28,608	0,313	4,289E-01
PANK4	21,568	21,250	0,318	6,192E-01
ACSF3	22,558	22,238	0,320	5,492E-01
SLC27A1	25,828	25,503	0,325	6,558E-01
ACTC1	30,865	30,528	0,337	5,789E-01
PFKL	27,468	27,128	0,340	5,191E-01
ROCK2	21,610	21,270	0,340	6,863E-01
SUMF2	26,235	25,885	0,350	5,431E-01
GNPDA1	24,165	23,800	0,365	7,674E-01
GAA	24,515	24,145	0,370	5,027E-01

CDIPT	25,733	25,360	0,372	3,732E-01
CDS2	24,993	24,613	0,380	4,958E-01
DEGS1	22,763	22,375	0,387	2,971E-01
SERINC1	23,023	22,623	0,400	4,176E-01
TRADD	21,042	20,632	0,409	6,571E-01
EIF2B1	24,098	23,685	0,412	5,169E-01
ALG12	21,448	21,036	0,413	6,181E-01
MLYCD	24,013	23,595	0,417	5,866E-01
APOA1	30,900	30,480	0,420	3,697E-01
CERS4	20,815	20,395	0,420	2,896E-01
ATP1B3	26,463	26,040	0,422	3,216E-01
ZMPSTE24	25,538	25,110	0,428	3,707E-01
ELOVL1	22,203	21,750	0,453	2,871E-01
CSNK2A1	27,303	26,845	0,458	2,973E-01
TPP2	20,866	20,403	0,463	5,714E-01
GNAI3	26,690	26,225	0,465	3,420E-01
AP2M1	27,298	26,830	0,467	2,527E-01
OSBPL8	23,870	23,403	0,467	2,739E-01
BDH2	24,268	23,800	0,467	5,762E-01
HRAS	24,505	24,033	0,472	3,194E-01
SLC25A12	24,808	24,335	0,472	3,057E-01
COPB1	26,385	25,913	0,473	5,484E-01
ACLY	23,675	23,200	0,475	6,793E-01
SPTLC1	23,398	22,915	0,483	2,322E-01
STAT1	25,950	25,458	0,493	4,316E-01
PFKM	21,854	21,351	0,503	6,654E-01
MB	20,354	19,840	0,514	3,349E-01
ARSD	23,008	22,490	0,518	3,750E-01
FDXR	23,438	22,918	0,520	2,431E-01
ALG1	21,892	21,372	0,520	2,629E-01
VDAC3	27,550	27,028	0,522	2,136E-01
TECR	29,193	28,663	0,530	2,827E-01
ACSL3	27,410	26,875	0,535	3,013E-01
ABCD3	23,928	23,390	0,537	2,199E-01
CALR	31,548	31,000	0,547	2,532E-01
NR3C1	19,813	19,264	0,549	3,675E-01
COPA	26,315	25,758	0,557	4,800E-01
CACNA2D1	29,680	29,113	0,567	2,016E-01
CLTC	29,645	29,073	0,572	3,323E-01
CPT1A	22,385	21,800	0,585	5,497E-01
MAP2K3	20,678	20,092	0,586	3,940E-01
PGM2	22,935	22,338	0,597	5,736E-01
DPM1	26,360	25,755	0,605	1,979E-01
SLC2A1	22,392	21,785	0,607	6,349E-01
AP2S1	25,680	25,073	0,608	1,618E-01

SLC1A5	25,230	24,620	0,610	1,312E-01
CANX	31,295	30,683	0,613	2,085E-01
GNAI2	30,325	29,700	0,625	1,598E-01
SACM1L	28,115	27,488	0,627	1,812E-01
FBP1	23,678	23,048	0,630	3,150E-01
PIP4K2A	23,038	22,403	0,635	1,606E-01
ALG2	23,595	22,955	0,640	1,025E-01
IDH2	29,333	28,690	0,643	1,983E-01
ME2	25,603	24,935	0,667	3,972E-01
SHMT2	24,360	23,690	0,670	3,134E-01
LRP1	29,908	29,238	0,670	1,170E-01
DPM3	24,243	23,570	0,672	1,376E-01
GNA11	28,700	28,018	0,682	1,864E-01
DOLPP1	22,315	21,623	0,693	2,389E-01
GNAS	29,458	28,740	0,717	1,264E-01
MICU1	20,311	19,590	0,721	2,059E-01
TPM3	29,088	28,360	0,727	1,881E-01
APOE	28,933	28,190	0,743	2,369E-01
MPDU1	25,863	25,118	0,745	9,698E-02
CAMK2D	24,433	23,688	0,745	5,675E-01
PI4K2A	22,875	22,128	0,747	1,302E-01
STIM1	24,935	24,178	0,758	1,838E-01
ATP2A2	28,628	27,868	0,760	1,590E-01
GM2A	22,595	21,833	0,762	1,586E-01
SLC25A20	28,680	27,905	0,775	1,138E-01
HACD2	27,880	27,098	0,783	2,516E-01
CA2	25,323	24,518	0,805	2,055E-01
NIPSNAP1	25,398	24,583	0,815	8,429E-02
HACD3	26,843	26,020	0,822	6,652E-02
LMAN2	28,353	27,530	0,823	4,972E-02
HEXB	24,335	23,490	0,845	3,591E-01
GOT2	26,125	25,280	0,845	5,826E-02
SLC39A7	25,933	25,083	0,850	7,764E-02
SLC25A13	25,613	24,755	0,857	9,936E-02
PCK2	26,583	25,715	0,867	3,268E-01
PRKACG	25,093	24,224	0,869	6,189E-01
GSR	24,743	23,865	0,878	3,617E-01
SLC27A3	23,958	23,063	0,895	1,105E-01
HEXA	23,358	22,430	0,928	4,077E-01
GGT1	24,045	23,108	0,938	7,498E-02
GDE1	23,328	22,349	0,978	2,612E-01
TPM1	24,883	23,900	0,982	2,579E-01
NAGK	26,188	25,203	0,985	1,825E-01
AGPAT1	21,845	20,845	1,000	2,648E-02
PPT1	23,815	22,815	1,000	5,805E-02

HBB	33,225	32,223	1,003	1,557E-01
ABCD2	24,280	23,260	1,020	1,571E-01
AGPS	25,013	23,978	1,035	5,669E-02
PITPNB	26,260	25,225	1,035	1,039E-01
SEC24C	22,814	21,740	1,074	3,334E-01
RPTOR	22,558	21,454	1,104	3,708E-01
GNA13	27,445	26,340	1,105	1,835E-02
GNAQ	27,898	26,770	1,128	4,301E-02
SLC3A2	28,243	27,103	1,140	4,426E-02
ADPGK	25,058	23,908	1,150	2,151E-02
HBB	23,085	21,925	1,160	2,465E-01
LMF2	24,653	23,488	1,165	1,924E-01
ATP1A2	21,043	19,860	1,183	2,667E-01
LPCAT3	25,613	24,420	1,193	1,589E-02
FAF2	26,448	25,210	1,238	4,833E-02
LPL	26,953	25,710	1,243	6,047E-02
FLOT1	29,355	28,093	1,263	9,666E-03
SGPL1	24,848	23,585	1,263	2,568E-02
MARCKS	25,815	24,530	1,285	3,148E-02
GYG1	23,600	22,303	1,297	2,577E-01
ALG9	21,539	20,230	1,308	2,007E-01
TPM4	27,108	25,795	1,313	4,736E-02
FTO	20,151	18,818	1,333	8,460E-02
CETP	22,283	20,895	1,388	2,944E-01
LBR	23,783	22,233	1,550	3,959E-03
FHL2	21,466	19,898	1,568	6,794E-02
FLOT2	28,985	27,415	1,570	1,921E-03
GPAM	29,103	27,513	1,590	1,747E-02
FTH1	30,675	29,048	1,627	2,952E-02
CERS2	23,558	21,928	1,630	4,586E-03
EBP	26,673	25,015	1,658	3,995E-03
GPD2	27,785	26,045	1,740	4,302E-03
FAAH	22,813	21,063	1,750	1,843E-02
TSTA3	22,605	20,803	1,802	4,971E-02
STS	24,490	22,675	1,815	6,994E-02
MBOAT7	21,657	19,817	1,839	6,207E-02
RENBP	21,822	19,949	1,873	5,151E-02
CISD2	26,440	24,495	1,945	2,256E-03
APOB	32,963	31,000	1,962	5,385E-02
APOA2	28,030	26,020	2,010	7,845E-03
PLD3	25,263	23,193	2,070	2,483E-03
BAX	22,540	20,457	2,083	1,378E-02
GSN	30,615	28,500	2,115	1,344E-03
ATP1A1	25,875	23,717	2,158	2,182E-01
LSS	30,078	27,870	2,208	4,347E-04

PON1	26,048	23,833	2,215	1,494E-02
HSD17B11	26,740	24,433	2,308	3,006E-03
APOC2	22,375	20,002	2,373	8,739E-02
APOC3	26,745	24,325	2,420	4,428E-02
ALB	33,525	31,055	2,470	9,886E-04
AGT	22,485	20,000	2,485	6,158E-03
SLC44A2	25,845	23,323	2,523	1,477E-03
ALDH3B1	24,705	22,160	2,545	3,735E-03
CALML5	22,247	19,691	2,556	3,496E-02
ALDH1A3	22,230	19,656	2,573	2,433E-02
LIPA	23,090	20,432	2,658	2,828E-03
MYL3	23,539	20,846	2,693	1,238E-01
STAT2	24,208	21,466	2,741	1,416E-02
ITPR1	24,040	21,073	2,967	1,057E-03
CYP1B1	22,454	19,444	3,010	1,825E-02
SERPINA5	21,955	18,943	3,012	2,390E-04
PLTP	23,656	20,610	3,046	9,504E-02
ARG1	24,455	21,233	3,223	4,346E-02
UBB	29,808	26,523	3,285	5,891E-03
A2M	29,603	26,253	3,350	1,408E-03
APOC4	25,763	22,380	3,383	6,086E-02
APOM	26,345	22,918	3,428	5,010E-03
ALOX5AP	24,353	20,849	3,503	2,028E-03
VTN	30,165	26,660	3,505	1,790E-03
PLG	25,163	21,618	3,544	2,126E-02
PTGS1	24,185	20,482	3,703	2,335E-04
RAC2	23,092	19,358	3,733	3,912E-03
ALOX5	22,758	18,994	3,764	7,134E-04
HSD17B7	23,150	19,384	3,766	2,950E-05
GMDS	22,397	18,631	3,766	2,509E-03
CTNNB1	23,310	19,526	3,784	5,420E-03
LEPR	26,410	22,589	3,821	4,565E-04
TBXAS1	23,670	19,704	3,966	2,679E-04
CIDEA	22,695	18,691	4,004	8,299E-04
AHSG	25,720	21,503	4,217	2,558E-03
FCER1G	24,295	20,024	4,271	1,277E-03
TTR	26,263	21,823	4,439	1,271E-04
TGM2	25,733	21,193	4,540	2,875E-04
APOC1	26,755	22,194	4,561	6,490E-03
NCEH1	25,235	20,393	4,842	1,341E-04
APOH	28,385	23,403	4,983	2,548E-05
GGT5	28,585	22,675	5,910	3,971E-05
RAF1	26,733	20,811	5,922	4,107E-05
CP	28,283	21,710	6,573	4,466E-05

1

Fig 1

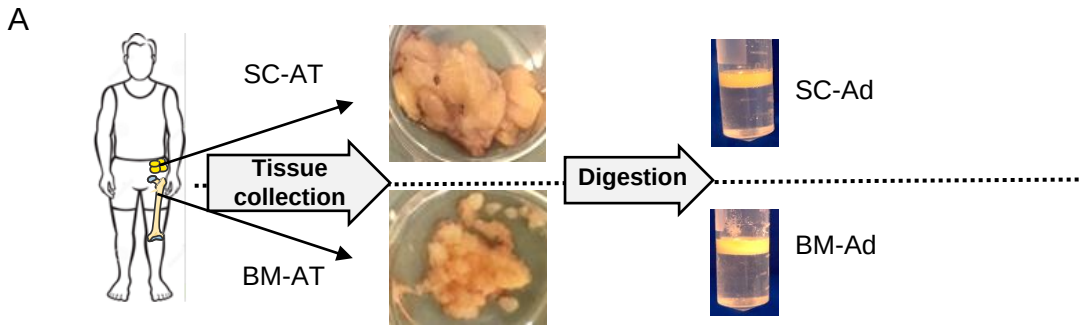
A
SC-AT
Tissue collection
BM-AT
Digestion
SC-Ad
BM-Ad

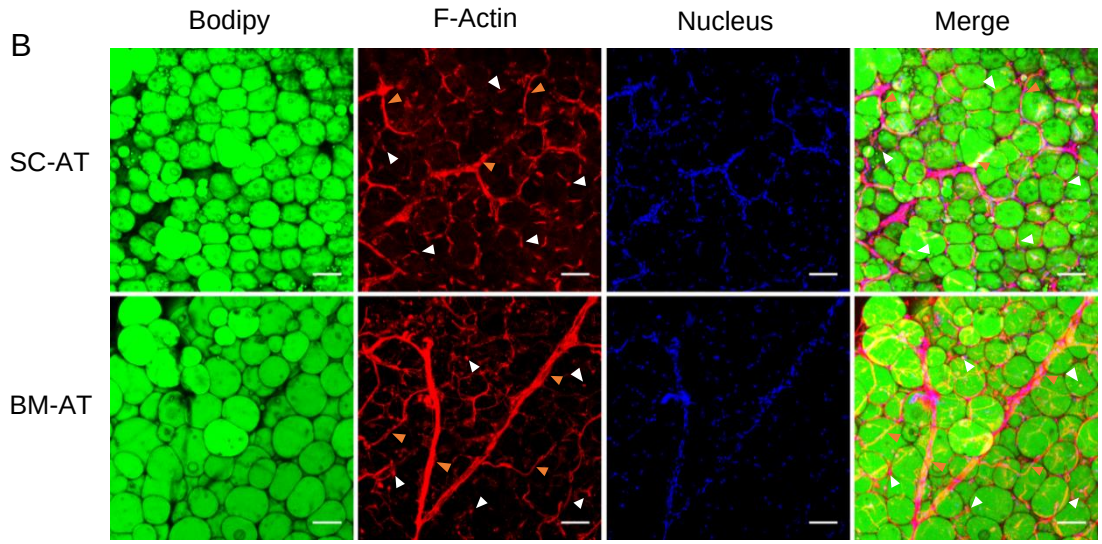
B
Bodipy
F-Actin
Nucleus
Merge
SC-AT
BM-AT

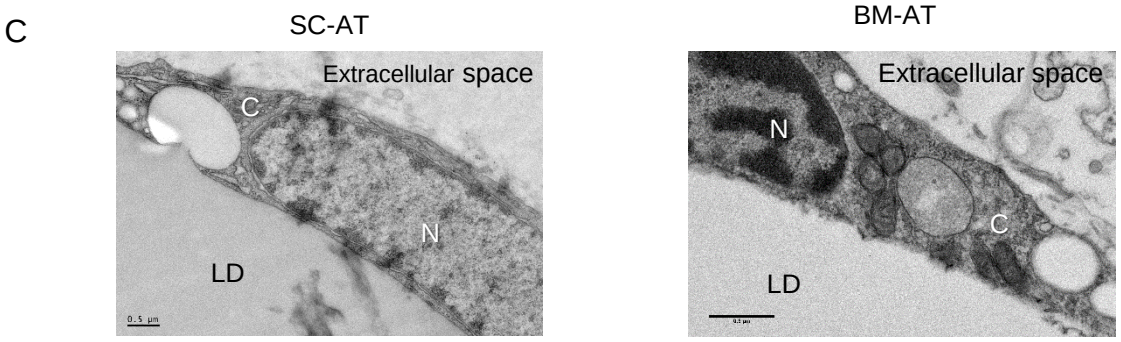
C
SC-AT
Extracellular space
C
N
LD
BM-AT
Extracellular space
N
C
LD

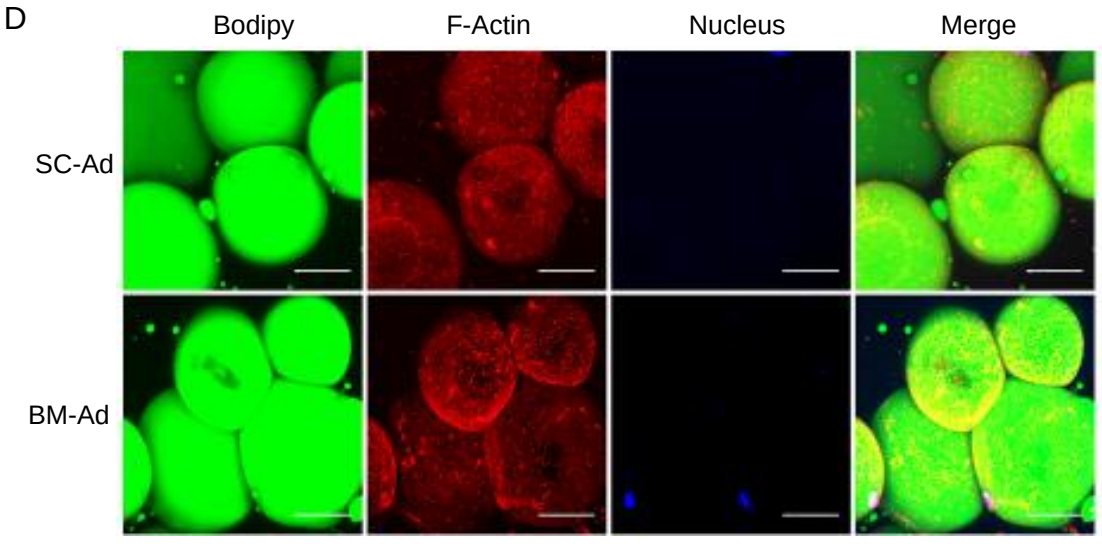
D
Bodipy
F-Actin
Nucleus
Merge
SC-Ad
BM-Ad

Fig EV1

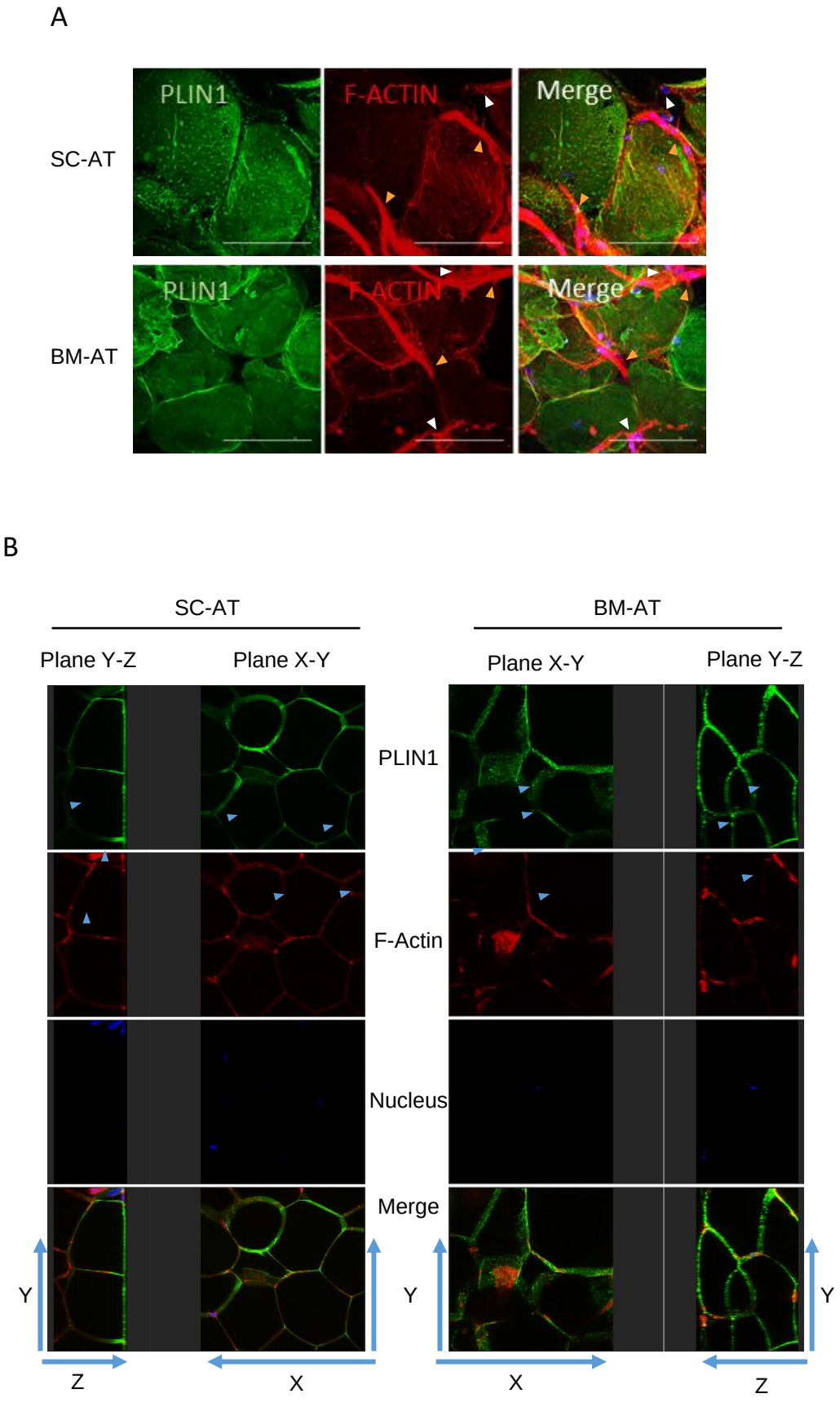
A
SC-AT
BM-AT
PLIN1
F-ACTIN
Merge
PLIN1
F-ACTIN
Merge
B
SC-AT
BM-AT
Plane Y-Z
Plane X-Y
Plane X-Y
Plane Y-Z
PLIN1
F-Actin
Nucleus
Merge
Y
Z
X
Y
X
Y
Z

Fig 2

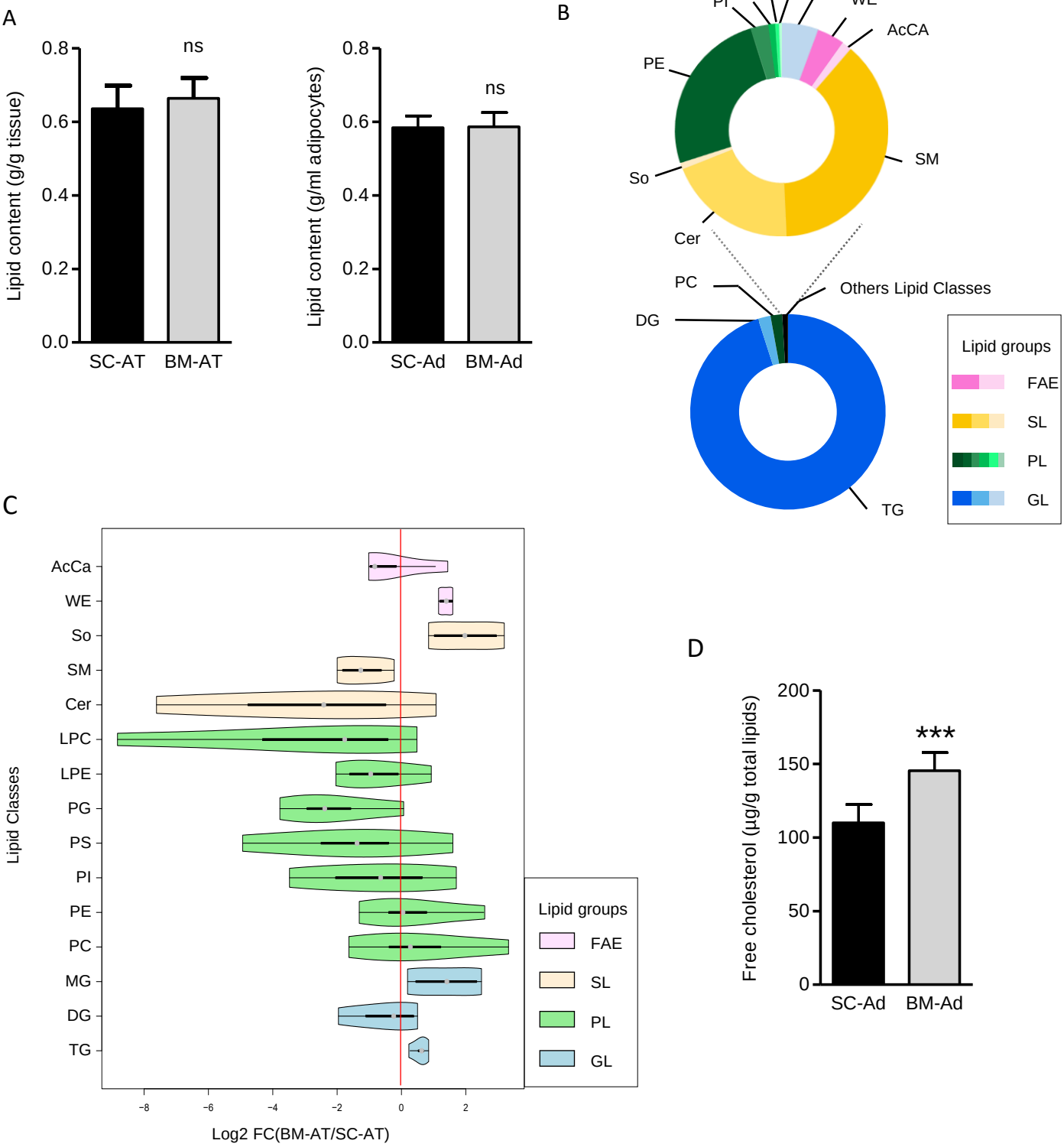
A
Lipid content (g/g tissue)
0.8
0.6
0.4
0.2
0.0
ns
SC-AT
BM-AT
Lipid content (g/ml adipocytes)
0.8
0.6
0.4
0.2
0.0
ns
SC-Ad
BM-Ad
B
LPC
PG
MG
PS
PI
WE
AcCA
PE
SM
So
Cer
PC
Others Lipid Classes
DG
TG
Lipid groups
FAE
SL
PL
GL
C
AcCa
WE
So
SM
Cer
LPC
LPE
PG
PS
PI
PE
PC
MG
DG
TG
Lipid Classes
−8
−6
−4
−2
0
2
Log2 FC(BM-AT/SC-AT)
Lipid groups
FAE
SL
PL
GL
D
Free cholesterol (µg/g total lipids)
200
150
100
50
0
***
SC-Ad
BM-Ad

Fig EV2

A

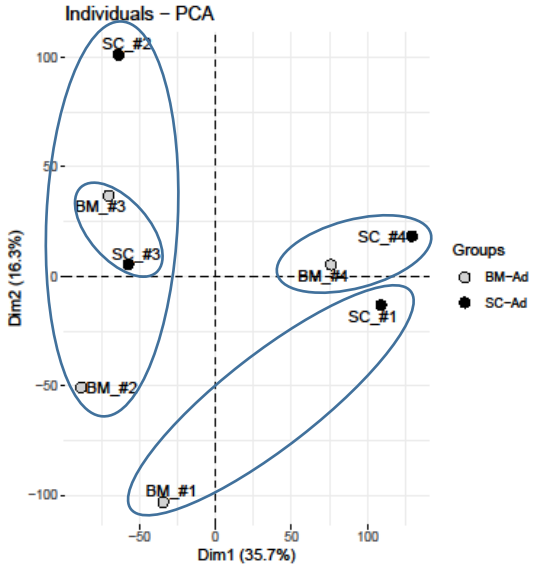
Individuals – PCA
SC_#2
BM_#3
SC_#3
SC_#4
BM_#4
SC_#1
BM_#2
BM_#1
Groups
BM-Ad
SC-Ad
Dim2 (16.3%)
Dim1 (35.7%)
100
50
0
−50
−100
−50
0
50
100

B

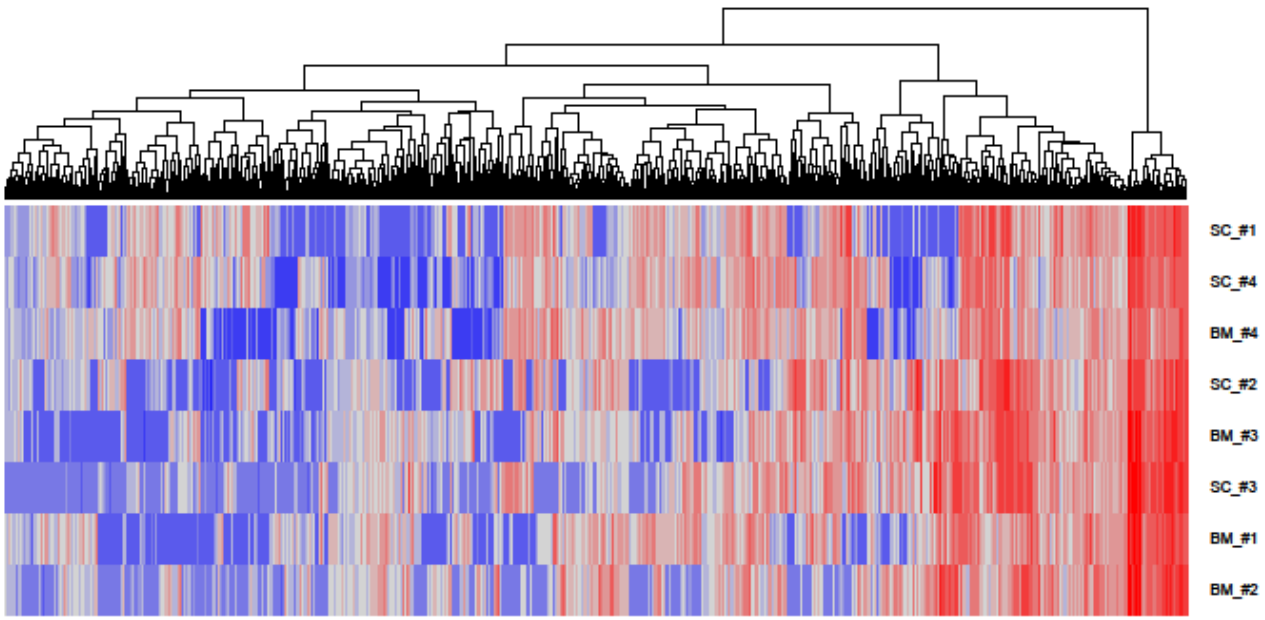
SC_#1
SC_#4
BM_#4
SC_#2
BM_#3
SC_#3
BM_#1
BM_#2

C

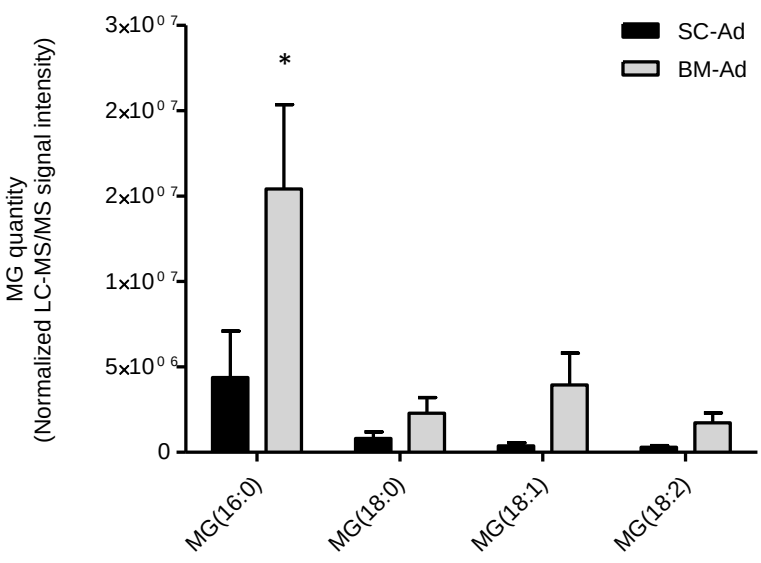
SC-Ad
BM-Ad
MG quantity
(Normalized LC-MS/MS signal intensity)
3x10^07
2x10^07
2x10^07
1x10^07
5x10^06
0
*
MG(16:0)
MG(18:0)
MG(18:1)
MG(18:2)

Fig 3

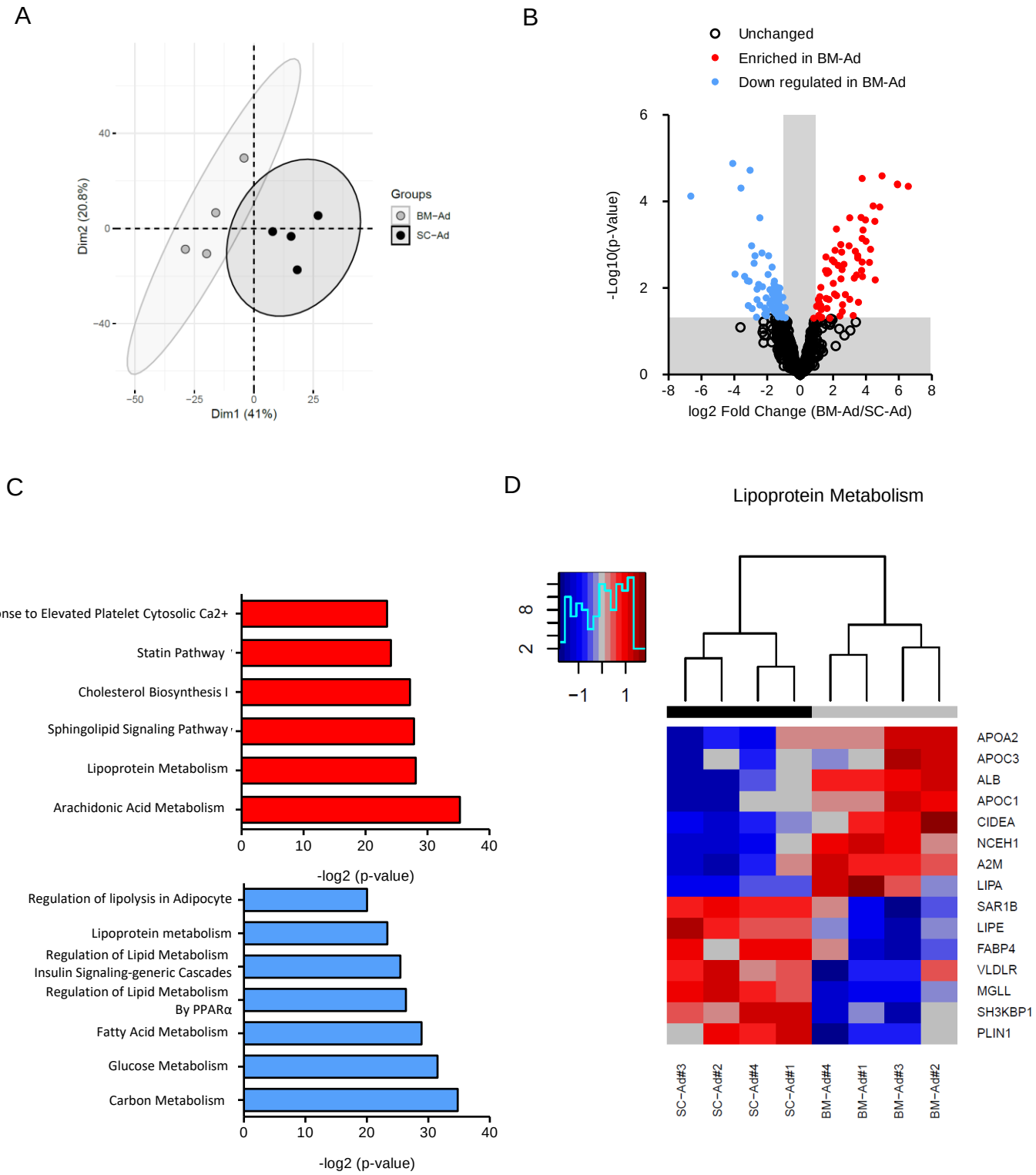
A
Dim2 (20.8%)
Dim1 (41%)
Groups
BM−Ad
SC−Ad
B
Unchanged
Enriched in BM-Ad
Down regulated in BM-Ad
-Log10(p-Value)
log2 Fold Change (BM-Ad/SC-Ad)
C
Response to Elevated Platelet Cytosolic Ca2+
Statin Pathway
Cholesterol Biosynthesis I
Sphingolipid Signaling Pathway
Lipoprotein Metabolism
Arachidonic Acid Metabolism
-log2 (p-value)
Regulation of lipolysis in Adipocyte
Lipoprotein metabolism
Regulation of Lipid Metabolism
Insulin Signaling-generic Cascades
Regulation of Lipid Metabolism
By PPARα
Fatty Acid Metabolism
Glucose Metabolism
Carbon Metabolism
-log2 (p-value)
D
Lipoprotein Metabolism
APOA2
APOC3
ALB
APOC1
CIDEA
NCEH1
A2M
LIPA
SAR1B
LIPE
FABP4
VLDLR
MGLL
SH3KBP1
PLIN1
SC−Ad#3
SC−Ad#2
SC−Ad#4
SC−Ad#1
BM−Ad#4
BM−Ad#1
BM−Ad#3
BM−Ad#2

Fig EV3

A

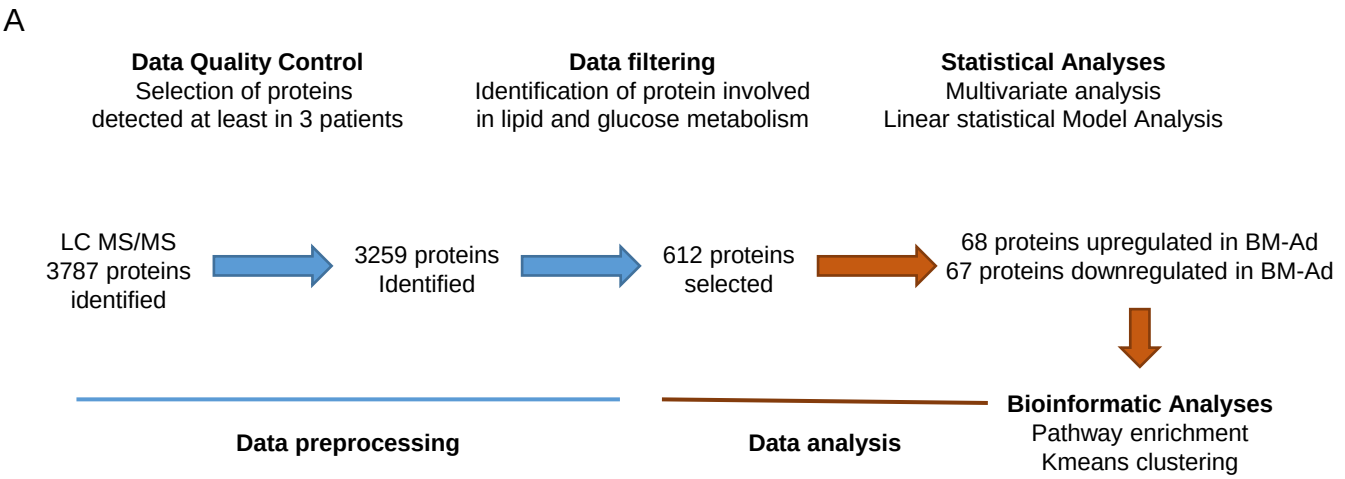

B

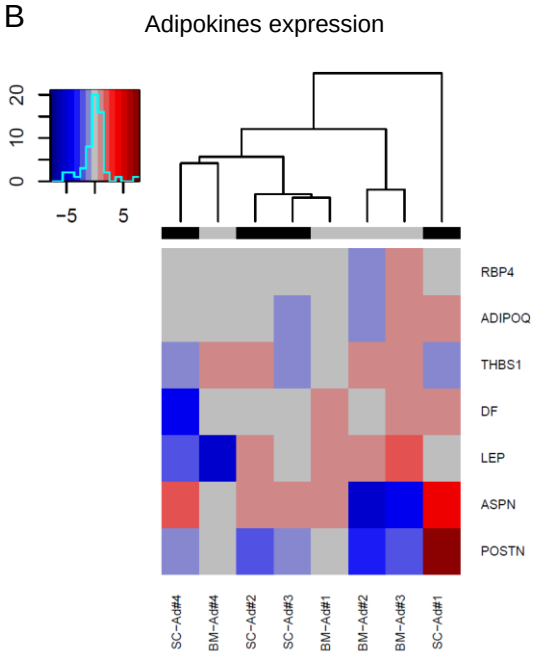

C

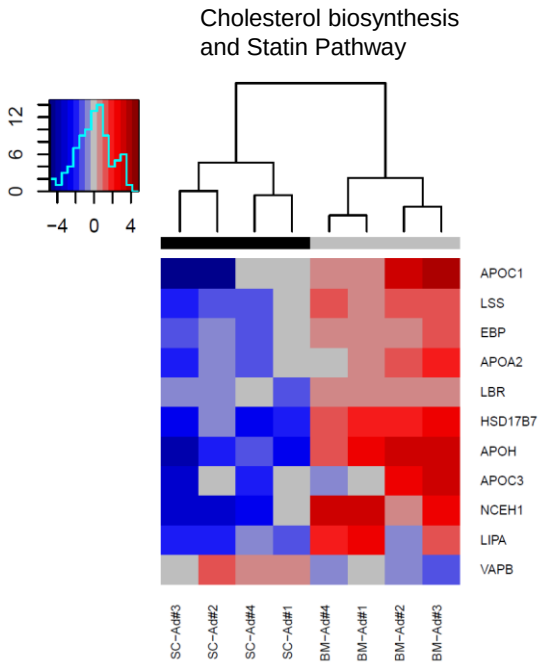

D

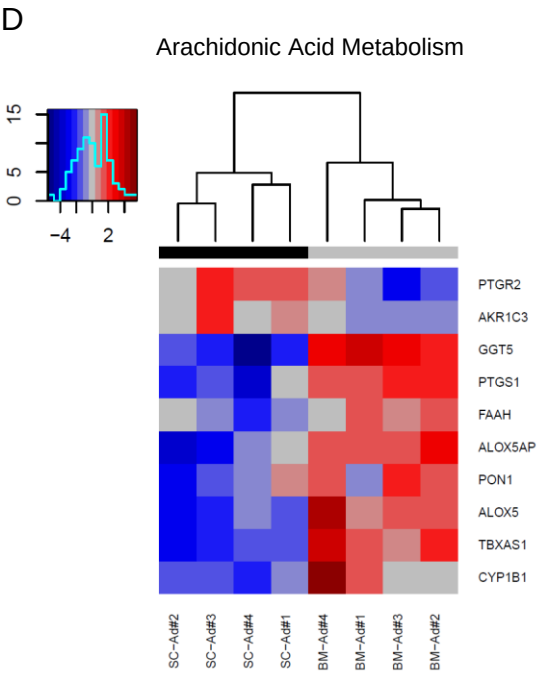

E

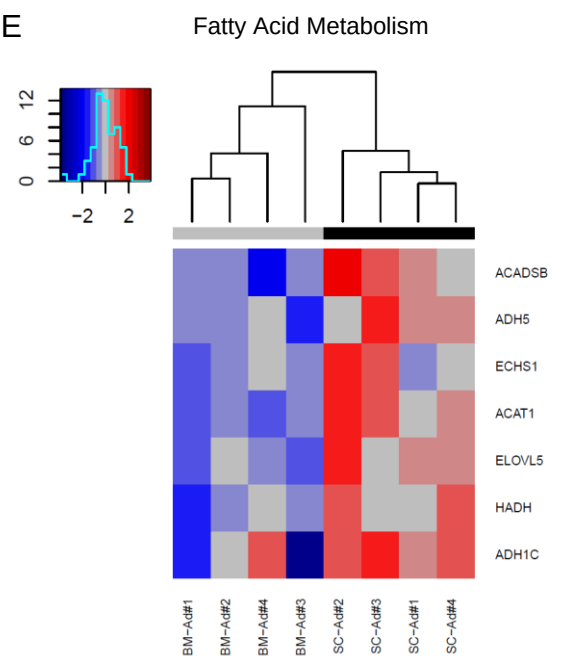

Fig 4

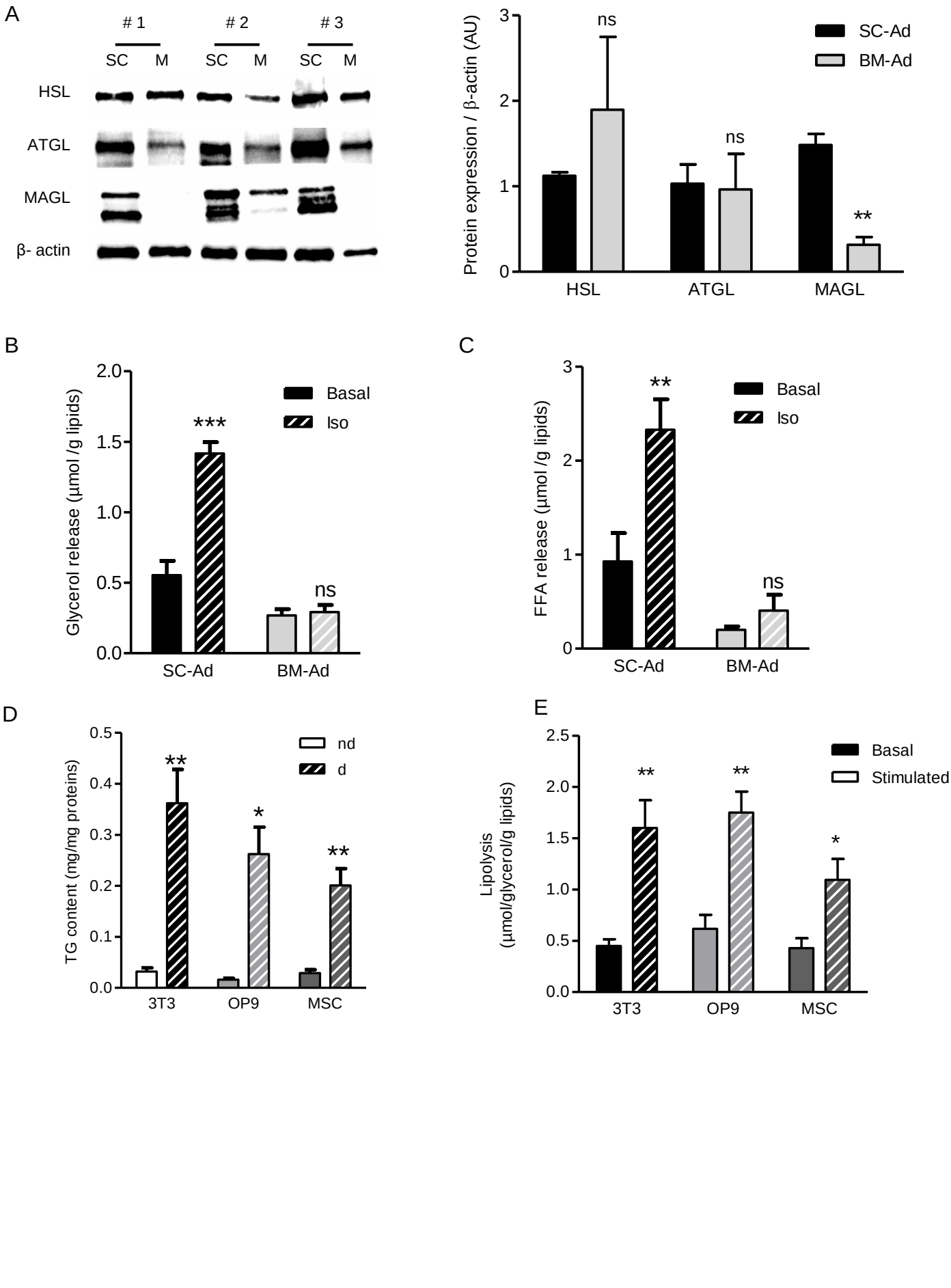
A
1
2
3
SC
M
SC
M
SC
M
HSL
ATGL
MAGL
β- actin
Protein expression / β-actin (AU)
ns
ns
**
SC-Ad
BM-Ad
HSL
ATGL
MAGL
B
Glycerol release (µmol /g lipids)
***
ns
Basal
Iso
SC-Ad
BM-Ad
C
FFA release (µmol /g lipids)
**
ns
Basal
Iso
SC-Ad
BM-Ad
D
TG content (mg/mg proteins)
**
*
**
nd
d
3T3
OP9
MSC
E
Lipolysis (µmol/glycerol/g lipids)
**
**
*
Basal
Stimulated
3T3
OP9
MSC